Journal of
Water & Climate Change

IWA PUBLISHING

Journal of Water and Climate Change Vol 16 No 12, 3886 doi: 10.2166/wcc.2025.211

A comparative impact assessment of using historical- and future-based flood hydrographs in planning flood control facilities

Emrah Yalcin * and Abdulselam Simsek

Department of Civil Engineering, Kirsehir Ahi Evran University, Kirsehir 40100, Turkey
*Corresponding author. E-mail: emrah.yalcin@ahievran.edu.tr

EY, 0000-0002-3742-8866; AS, 0000-0002-9845-2229

ABSTRACT

Climate change highlights the need for regional assessments to enhance flood mitigation planning. This study presents an integrated framework for evaluating the effectiveness of a detention reservoir, designed using historical precipitation data, in mitigating flood risks over an urban floodplain, with Hastane Brook in Kirsehir (Turkey) as a case study. Precipitation simulations from 10 global circulation models (GCMs) under the Coupled Model Intercomparison Project Phase 6 (CMIP6) are used to synthetically project 500-year return period flood hydrographs for both the CMIP6 historical experiment and the Shared Socioeconomic Pathway (SSP) scenarios SSP2-4.5 and SSP5-8.5. Four different probability distribution functions are applied to estimate rainfall magnitudes for the historical (1950–2014) and future (2025–2099) periods. Climate change impacts are quantified based on the medians of the 500-year recurrence rainfall amounts derived from the precipitation data of each GCM, using the best-fitted distribution functions according to the Kolmogorov–Smirnov test results. Flooding impacts are analyzed using a two-dimensional hydrodynamic model developed in HEC-RAS 6.5 software. The results raise concerns, as projections indicate an 18.3% increase in the 500-year rainfall amount under the SSP5-8.5 scenario, suggesting that the detention reservoir's capacity may be insufficient if climate change follows this high-forcing pathway.

Key words: 2D hydrodynamic modeling, climate change, CMIP6, flood control, HEC-RAS, urban flooding

HIGHLIGHTS

- A framework is proposed to assess the adequacy of a detention reservoir designed using historical precipitation data under the SSP2-4.5 and SSP5-8.5 scenarios.
- While the reservoir capacity remains sufficient under the SSP2-4.5 scenario, its effectiveness declines under the SSP5-8.5 scenario.
- Raising the 23 m high dam by only 1.5 m could restore the reservoir's flood mitigation effectiveness under the SSP5-8.5 scenario.

1. INTRODUCTION

Flooding is regarded as one of the most devastating natural hazards. A major concern is the increasing likelihood of floods, particularly in urban areas with dense populations and valuable assets (Huong & Pathirana 2013; Rosbjerg 2017; Jiang *et al.* 2018; Zhou *et al.* 2018; Yadav *et al.* 2024). Climate change and urban growth are key drivers of rising flood risks, posing significant challenges for both current and future flood management strategies (Mahmood *et al.* 2017; Skougaard Kaspersen *et al.* 2017; Wu *et al.* 2017; Arnone *et al.* 2018). Alterations in climate patterns disrupt the hydrological cycle and intensify extreme precipitation events, leading to greater surface runoff and more frequent floods (Karamouz *et al.* 2011; Mahmoud & Gan 2018; Pathak *et al.* 2020). Although floods are naturally occurring extreme hydroclimatic events, their destructive impact is exacerbated by poor land-use planning, neglect of riverine ecosystems, and uncontrolled development in flood-prone areas (Mileti & Gailus 2005; Abdi-Dehkordi *et al.* 2021). With continued urban expansion and the ongoing effects of climate change, flood risks are expected to rise in many regions worldwide (Jongman *et al.* 2012; Hirabayashi *et al.* 2013; Schoppa *et al.* 2024). If flood vulnerability remains unchanged, global annual flood-related losses could increase tenfold by the end of the century (Winsemius *et al.* 2016; Alfieri *et al.* 2018; Dottori *et al.* 2018).

The mitigation of vulnerability through flood adaptation has historically proven effective and remains a fundamental strategy for addressing the anticipated rise in flood-related impacts (Jongman *et al.* 2015; Tanoue *et al.* 2016; Winsemius *et al.* 2016; Jongman 2018; Kinoshita *et al.* 2018; Schoppa *et al.* 2024). While structural measures, such as building dams and levees and increasing channel capacity, play a crucial role in reducing flood impacts by lowering peak discharge and flood volume, they cannot be relied upon solely for larger and more frequent flood events in the future (Lawler 2009; Kundzewicz & Stakhiv 2010; Wilby & Keenan 2012). Similarly, non-structural measures, such as developing early warning systems and establishing reservoir operation rules, are not standalone solutions under changing climate conditions (Jamrussri & Toda 2017; Abdi-Dehkordi *et al.* 2021). Hence, a deeper understanding of the evolving drivers of flood risks is essential for developing adaptive and forward-looking mitigation strategies that integrate both structural and non-structural measures. However, many existing studies primarily rely on statistical analyses of historical rainfall intensity and frequency when developing adaptation measures. These practices assume that hydrological parameters remain constant over time, overlooking potential variability (Bhusal *et al.* 2024).

A widely used approach to projecting climate change impacts involves integrating climate simulations from global circulation models (GCMs) with downscaling techniques or high-resolution regional circulation models (RCMs) (Prudhomme *et al.* 2010; van Roosmalen *et al.* 2010; Teutschbein & Seibert 2012; Yadav *et al.* 2024). The Coupled Model Intercomparison Project (CMIP), a collaborative initiative under the World Climate Research Program, consolidates climate models to refine projections on hydroclimatological variables, such as precipitation, temperature, and runoff, under several climate scenarios. Its latest phase, CMIP6, employs Shared Socioeconomic Pathways (SSPs), which replace the previous Representative Concentration Pathways (RCPs). SSPs integrate societal development trends with anthropogenic influences, such as greenhouse gas emissions and land-use changes, to provide more comprehensive climate impact assessments (O'Neill *et al.* 2016). Variations in simplifications, parameterizations, and numerical approximations of climate systems across different GCMs introduce model uncertainty in long-term hydroclimatological projections (Murphy *et al.* 2004; Knutti *et al.* 2010). Several methods have been proposed to assess and mitigate uncertainty associated with GCM selection (Shiogama *et al.* 2016; Hosseinzadehtalaei *et al.* 2017; Mateus & Tullos 2017; Kaczmarska *et al.* 2018; Lehner *et al.* 2019). Although many of these approaches compare individual GCMs to their ensemble mean, it is crucial to recognize that the return period of extremes is more influenced by climate variability than climatic mean (Salman *et al.* 2020). Wang *et al.* (2020) suggested using a minimum of 10 GCMs to evaluate climate change impacts on hydrology.

Kirsehir Province, located in the Central Anatolia Region of Turkey, is particularly vulnerable to flood hazards in the northeastern part of its city center. This vulnerability stems from Hastane Brook, an intermittent stream that originates in the mountainous terrain north of the city. Hastane Brook flows sporadically for only a few days each year, draining an 11.1 km^2 catchment area before reaching the urban environment, as shown in Figure 1. Historically, the natural flow path of Hastane Brook toward Kilicozu Creek was obstructed by the construction of the Ankara-Kayseri intercity road. Subsequent urban expansion, including the development of roads and buildings within the flood-prone area, has completely eliminated the streambed. As a result, during potential flood events, runoff from the semi-arid mountainous watershed is expected to bypass the intercity road and directly inundate the city center. To mitigate the flood risk posed by Hastane Brook, local authorities have argued for a detention dam project within the Hastane basin at an elevation of approximately 1,068 m, as illustrated in Figure 1. This scheme is intended to temporarily impound floodwaters in a detention reservoir and divert bottom outlet releases through a transmission channel that passes over the urban core before discharging into Kilicozu Creek. The storage capacity of the planned detention reservoir will be traditionally determined based on a 500-year recurrence flood hydrograph derived from historical records. However, climate change presents a significant challenge, as an increase in flood hydrograph volume could exceed the reservoir's design capacity. In such a case, excess floodwaters would be discharged via an uncontrolled overflow spillway, leading to the inundation of the city center despite this structural measure.

This study aims to evaluate the potential impacts of climate change on the future effectiveness of a flood control structure designed using synoptic station records. The evaluation is based on precipitation projections from GCMs belonging to the CMIP6 database, with a focus on the Hastane Brook basin and its floodplain in the city center of Kirsehir. To assess the changing climate impacts, 500-year recurrence rainfall amounts for the Kirsehir meteorological station (MS) (Figure 1) are projected using precipitation data from 10 CMIP6 GCMs under the medium- and high-forcing SSP scenarios of SSP2-4.5 and SSP5-8.5 (O'Neill *et al.* 2016) over the 2025–2099 period. For each future scenario, the analysis relies on the median of the rainfall magnitudes derived from the precipitation data of each GCM, comparing them with a baseline scenario

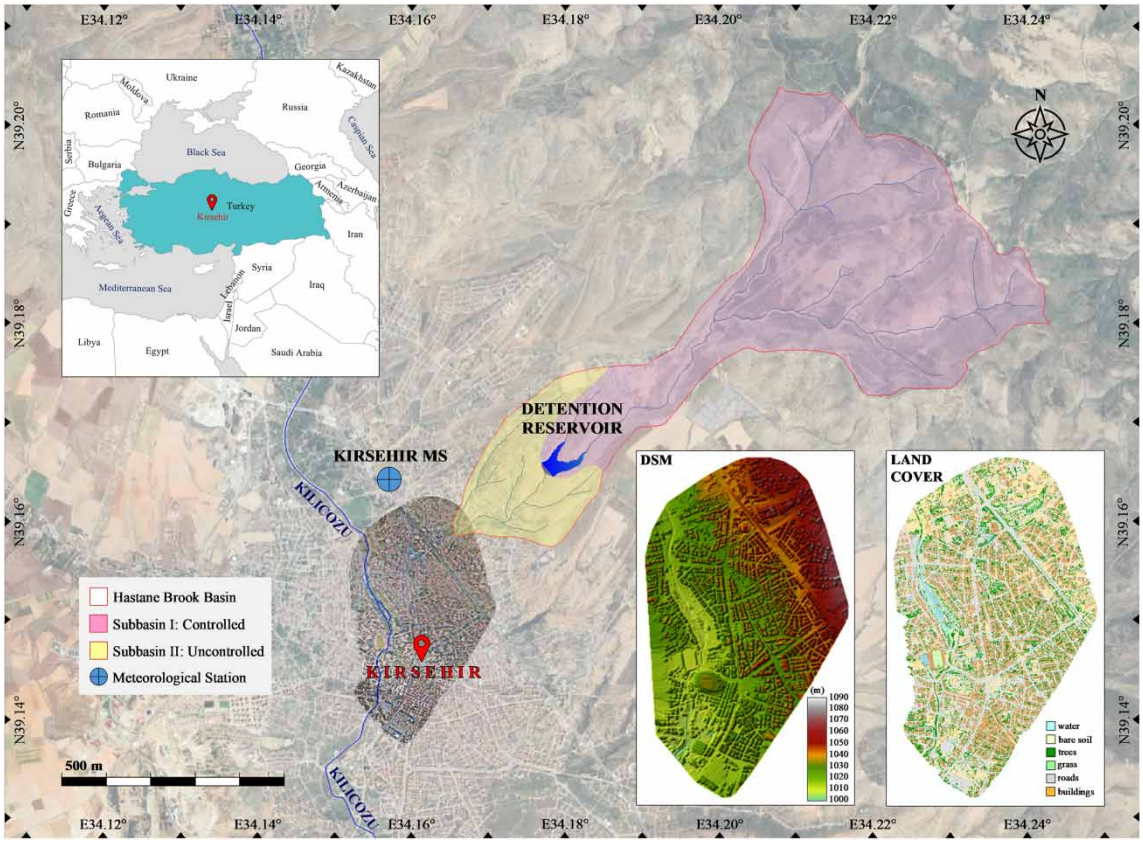

Figure 1 | Details of the study area.

established using the median rainfall magnitude from the CMIP6 historical experiment (O'Neill *et al.* 2016) for the period from 1950 to 2014. The study follows a structured four-step methodology: (1) estimation of 500-year flood hydrographs for the Hastane Brook basin and its subbasins using precipitation records from the Kirsehir MS and design of the detention reservoir project, (2) generation of 500-year flood hydrographs for the basin and subbasins using bias-corrected precipitation simulations from CMIP6 GCMs, (3) development of a two-dimensional (2D) hydrodynamic flood routing model using HEC-RAS 6.5 by incorporating a high-resolution digital surface model (DSM) and land cover data derived from unmanned aerial vehicle (UAV) photogrammetry for the urban floodplain, and (4) evaluation of the detention reservoir's effectiveness under projected climate scenarios by assessing its capacity to mitigate flooding if climate change follows medium- or high-forcing pathways. By highlighting the increasing flood risks posed by future climate change, this study underscores the importance of integrating climate resilience into flood control infrastructure planning and management for the Hastane Brook basin, while providing a comprehensive framework for adaptive mitigation strategies applicable to other basins facing similar hydrological challenges.

2. STUDY AREA AND UTILIZED DATASETS

2.1. Description of the study area

The flood-prone region is estimated to encompass an area of 3.2 km^2, constituting about 60% of the urban core of Kirsehir (Figure 1). This densely populated and infrastructurally critical zone includes essential facilities such as hospitals, schools, playgrounds, government institutions, and mosques, all integral to the city's daily functioning. After traversing the city center, floodwaters are projected to discharge into Kilicozu Creek. The most recent major flooding event from Hastane Brook occurred in 1989, resulting in the submergence of roads and ground floors in 20 buildings, as documented in the preliminary investigation report on flood mitigation strategies for the Kirsehir city center (DSI 1989). The report recommended diverting the stream into a channel extending to Kilicozu Creek. However, neither structural nor non-structural measures

have been implemented to address the recurrent flooding risks, and urbanization in the area has continued unabated. Moreover, like other parts of the city center, the floodplain lacks an adequate stormwater drainage system. Beyond the findings of this report, no comprehensive flood data, including flood hydrographs, inundation depths, and flooding extents, have been recorded (SYGM 2019). Even if such data were available, their relevance to current flood risk assessments would be questionable due to significant changes in the topography of the flood-prone area. For instance, in 1979, the natural sections of Kilicozu Creek within the urban area were replaced by a rectangular concrete channel. Later, in 2014, the Kentpark recreational project was undertaken along an approximately 800-m section of the channel, beginning at the creek's urban entry point. This project replaced the existing rectangular cross-section of 10 m by 3.5 m with a newly designed channel featuring variable dimensions, ranging from 10 to 88 m in width and 1.3 to 4.7 m in depth (Sigal 2012). Moreover, the Hastane overpass on the Ankara-Kayseri road, constructed in 2015, has the potential to influence the hydrodynamic behavior of floodwaters toward the urban core.

2.2. Hydroclimate datasets

The 500-year recurrence interval flood scenarios for the city center of Kirsehir are constructed based on 65 years of daily precipitation records (1950–2014) from the Kirsehir MS (Station ID: 17160), managed by the Turkish State Meteorological Service (MGM) (Figure 1) (MGM 2024a, b). The lack of other *in-situ* stations within or near the Hastane Brook basin prevents the calculation of mean areal precipitation for the watershed. Flood hydrographs for the Hastane basin are estimated using the superposed Mockus and DSI synthetic unit hydrograph techniques, which fundamentally differ in their computational frameworks for determining parameters such as peak discharge, time to peak discharge, and base time. Snyder's method is deemed inapplicable because the catchment area is less than 1,000 km^2 (Ozdemir 1978; Usul 2009). Additionally, the absence of representative stream gauging stations in or near the basin necessitates excluding the statistical estimation of flood peaks from runoff data through point or regional flood frequency analyses, thereby relying on synthetic methods.

Daily precipitation simulations from 10 CMIP6 GCMs at the coordinates of the Kirsehir MS are used to generate 500-year recurrence flood hydrographs for the Hastane Brook basin under the CMIP6 historical experiment and the medium- and high-forcing future scenarios of SSP2-4.5 and SSP5-8.5. The flooding scenario derived from the CMIP6 historical experiment is crucial for evaluating its alignment with computations based on the *in-situ* station records and for establishing a baseline scenario to assess the impacts of future climate on flooding risks. The grid-based GCM datasets are sourced from the Earth System Grid Federation (ESGF) platform (ESGF 2022). Table 1 provides details of the selected GCMs, including model

Table 1 | Overview of the GCMs considered in the study

Model ID	Institution	Spatial resolution in arc degrees (latitude x longitude)
ACCESS-CM2	Commonwealth Scientific and Industrial Research Organization (CSIRO) & Australian Research Council Centre of Excellence for Climate System Science (ARCCSS), Australia	1.25° × 1.875°
CMCC-ESM2	Centro Euro-Mediterraneo sui Cambiamenti Climatici (CMCC), Italy	0.9424084° × 1.25°
EC-Earth3	EC-Earth Consortium, Europe	(0.696–0.702)° × 0.703125°
EC-Earth3-CC	EC-Earth Consortium, Europe	(0.696–0.702)° × 0.703125°
EC-Earth3-Veg	EC-Earth Consortium, Europe	(0.696–0.702)° × 0.703125°
KIOST-ESM	Korea Institute of Ocean Science and Technology (KIOST), Korea	1.875° × 1.875°
MPI-ESM1-2-HR	Max Planck Institute for Meteorology (MPI-M) and Deutsches Klimarechenzentrum (DKRZ), Germany	(0.927–0.935)° × 0.9375°
NorESM2-LM	NorESM Climate Modeling Consortium, Norway	1.894737° × 2.5°
NorESM2-MM	NorESM Climate Modeling Consortium, Norway	0.9424084° × 1.25°
TaiESM1	Research Center for Environmental Changes – Academia Sinica (AS-RCEC), Taiwan	0.9424084° × 1.25°

identifiers, affiliations, and spatial resolutions. The selection criteria prioritize the availability of daily precipitation data for the first ensemble member (r1i1p1f1) of each GCM across the targeted climate scenarios. Furthermore, before extracting raw simulation data at the station coordinates, climate datasets with varying grid resolutions are standardized to a spatial resolution of 0.5° × 0.5° using the first-order conservative remapping method (Jones 1999).

Based on long-term records from the Kirsehir MS, the mean annual number of days with snow cover is approximately 37, while the average monthly snow depth from November to March is only 7 cm (MGM 2024c). Thus, snowmelt contributes negligibly to runoff within the watershed. Periodic site investigations conducted over 8 years have also revealed the absence of continuous water flow in Hastane Brook throughout the year, a finding corroborated by interviews with residents. Consequently, neither baseflow nor snowmelt runoff is included in the estimated flood hydrographs for the 2D hydrodynamic flood analyses. Similarly, for the Kilicozu Creek watershed, snowmelt is considered to have an insignificant impact on runoff (MGM 2024c, d). Therefore, a constant baseflow rate of 3.34 m^3/s, calculated by Yalcin (2020), is used as the inflow hydrograph at the point where the creek enters the city (Figure 1). This rate is uniformly applied across all historical and future climate scenarios.

2.3. Topographic mapping and land cover-related datasets

The topographical parameters essential for deriving synthetic unit hydrographs, including drainage area, hydraulic length of the basin, distance from the basin outlet to the point on the mainstream nearest to the basin centroid, and harmonic slope of the mainstream, are obtained from the 1:25,000 scale digitized topographic maps of the region. The dimensions of the proposed detention dam are determined using the 1:1,000 scale digitized topographic map of the project area, which also provides details about reservoir characteristics. The high-resolution DSM generated by Yalcin (2018) using UAV-based aerial photography serves as the base topographic data for the presumed flood-prone area (Figure 1). This source DSM was created with a ground sampling distance of 4.32 cm/pixel from 2,216 geo-referenced images captured during UAV flights over the Hastane Brook floodplain. To enhance geolocation accuracy, 30 ground control points with known geographic coordinates were used during image processing. The absolute accuracy of the DSM was validated using the geodetic coordinates of three additional checkpoints, yielding root mean square error (RMSE) values of 5.1 cm horizontally and 12.7 cm vertically. Additionally, the orthophoto of the floodplain, prepared by Yalcin (2018) through the integration of geometrically corrected aerial images, is utilized for classifying land cover types within the study area (Figure 1). This classification enables the assignment of Manning's roughness (n) values to the identified land features, thereby supporting the hydrodynamic modeling process.

3. METHODOLOGY

3.1. Determination of 500-year flood hydrographs using the station records

The 500-year historical flood scenario for the Hastane Brook basin is constructed using the superposed Mockus and DSI synthetic unit hydrograph methods, based on annual maximum 24-h precipitation data from the Kirsehir MS. The process begins with determining the 500-year recurrence daily rainfall rate at the Kirsehir station through the log-Pearson type 3 frequency distribution, considering the results of the non-parametric Kolmogorov–Smirnov (K-S) test (McCuen 1993) for the log-normal (with two parameters), log-normal (with three parameters), log-Pearson type 3, and Gumbel distributions. The critical precipitation duration for the region is identified as 4 h (Ozdemir 1978). Subsequently, the corrected and maximized 500-year rainfall magnitude for the basin is calculated by multiplying the 500-year recurrence daily rainfall rate with the 4-h pluviograph coefficient from the Kirsehir station, the 4-h areal precipitation distribution coefficient specific to the basin, and a maximization factor of 1.13 (Ozdemir 1978; Eren 2011). Topographical parameters are incorporated into the synthetic methods to generate 0.5-h unit hydrographs, which differ in terms of peak discharge, time to peak, and base time. For each method, the 500-year rainfall magnitude over the critical 4-h duration is divided into 0.5-h rainfall blocks using the regional time distribution curve of precipitation. The SCS method is then applied to separate initial abstraction and actual retention from rainfall, enabling the computation of excess rainfall (or direct runoff) for each 0.5-h interval (Ozdemir 1978; Ponce & Hawkins 1996; Usul 2009). Finally, 500-year recurrence flood hydrographs are derived using the unit hydrograph method, incorporating the 0.5-h synthetic unit hydrographs and the incremental excess rainfall depths (Ozdemir 1978; Dernek 2012). Among the methods, the superposed Mockus method, which predicts the highest peak discharge, is prioritized during the hydrodynamic modeling phase of the study to ensure a conservative approach in delineating flood risk zones within the city center.

The derivation of the design inflow hydrograph is essential for designing a detention facility. To determine the flood discharges needed for sizing the proposed detention reservoir project, which consists of an embankment dam and an uncontrolled overflow spillway, and to reevaluate flood risks in the Kirsehir city center after the construction of the detention scheme, the Hastane Brook basin is analyzed in two subbasins. These subbasins are the flood detention catchment (subbasin 1) and the intermediate catchment between the dam site and the Hastane basin outlet (subbasin 2), as shown in Figure 1. The drainage areas of subbasin 1 and subbasin 2 are 9.36 and 1.74 km^2, respectively. Accordingly, topographic parameters and 4-h areal precipitation distribution coefficients are determined for both subbasins, and the recurrence flood hydrographs are generated using synthetic unit hydrographs with 0.5-h intervals, employing the superposed Mockus and DSI methods. Similar to the Hastane basin, the superposed Mockus method yields the highest peak discharge values for both subbasins. The 500-year flood hydrograph volume for the detention catchment, estimated with the superposed Mockus method, is then used to determine the required reservoir storage and, consequently, the crest elevation of the embankment. The capacity and dimensions of the overflow spillway are designed based on the 10,000-year flood discharge, also estimated with the superposed Mockus method. The key features of the proposed detention reservoir project are listed in Table 2. Since there will be no spillway outflow under the 500-year historical flooding scenario, only the 500-year recurrence flood hydrograph generated for subbasin 2 is utilized as input data in the hydrodynamic model run for the historical scenario involving the construction of the project.

Table 2 | Salient features of the detention reservoir project dimensioned based on the records of the Kirsehir MS

Item	Unit	Value
General		
Type	–	Homogeneous clay fill
Drainage area	km^2	9.36
Reservoir		
Maximum water level	m	1,089.47
Minimum water level	m	1,079
Total volume at the maximum water level	hm^3	0.359
Active storage	hm^3	0.241
Dead storage	hm^3	0.051
Reservoir area at the maximum water level	km^2	0.049
Reservoir area at the minimum water level	km^2	0.014
Dam embankment		
Upstream and downstream side slopes	–	3H/1V and 2.5H/1V
Thalweg elevation	m	1,068
Crest elevation	m	1,091
Crest length	m	199
Crest width	m	8
Height of dam above thalweg	m	23
Spillway		
Type	–	Uncontrolled overflow
Design discharge ($Q_{10,000}$)	m^3/s	50.96
Entrance channel bottom elevation	m	1,087
Sill height	m	1
Crest elevation	m	1,088
Crest length	m	12
Design water head	m	1.47

3.2. Determination of 500-year flood hydrographs using the GCM simulations

3.2.1. Bias correction of the GCM datasets

Bias adjustment is essential for GCM simulations to address systematic errors and ensure alignment with observed climate characteristics, such as distribution, sequencing, and magnitude (Tan *et al.* 2020). Accordingly, the GCM datasets corresponding to the coordinates of the Kirsehir MS are subjected to bias correction using daily precipitation records from the station as a reference. This process employs the distribution mapping (DM) method, implemented within the Climate Model Data for Hydrologic Modeling (CMhyd) tool (Rathjens *et al.* 2016), to mitigate potential systematic biases at the local scale for both historical 1950–2014 and future 2025–2099 periods. Unlike simple adjustments to the mean and variance of GCM data, the DM method modifies the distribution function of GCM simulations based on the distribution of observed data (Wang & Chen 2014). This makes it particularly suitable for analyzing recurrence intervals and extreme precipitation events. Several studies have highlighted DM as one of the most effective bias correction approaches compared with alternative methods (Teutschbein & Seibert 2012; Zhang *et al.* 2018). More recent methods, such as multivariate bias correction techniques (Cannon *et al.* 2015; Cannon 2018), are advantageous for preserving inter-variable and inter-site dependencies; however, this study focuses specifically on univariate precipitation extremes at the basin scale. Although the DM method assumes stationarity of bias and may have limited extrapolation capability under unprecedented extremes, the study region has historically not experienced such extremes and is projected to remain so in the future (Tugrul *et al.* 2025). The modified index of agreement (*md*) (Legates & McCabe 1999), normalized RMSE (nRMSE) (Almeida *et al.* 2015), Kling–Gupta efficiency (KGE) (Gupta *et al.* 2009), and percent bias (PBIAS) metrics are used to evaluate the performance of the bias-corrected historical GCM simulations on a monthly scale.

3.2.2. Precipitation frequency analysis

Annual daily precipitation peaks are extracted from the bias-corrected daily simulations of each GCM under the CMIP6 historical experiment, as well as the medium- and high-forcing future scenarios of SSP2-4.5 and SSP5-8.5, to perform precipitation frequency analysis. Recurrence rainfall amounts, calculated from the annual maximum daily precipitation time series of the GCMs under the CMIP6 historical experiment for the 1950–2014 period, serve as the baseline, while future changes in these recurrence rainfall amounts are evaluated using the simulated peaks from the 2025–2099 period under the future scenarios. Although the study primarily focuses on 500-year recurrence flood events, rainfall amounts for the 5-, 10-, 25-, 50-, and 100-year return periods are also analyzed to assess the performance of the selected 10 GCMs in simulating annual maximum daily precipitation. The first step in the analysis involves conducting the non-parametric K-S test for each set of annual daily precipitation peaks to evaluate the appropriateness of the considered distribution functions (i.e., log-normal (with two parameters), log-normal (with three parameters), log-Pearson type 3, and Gumbel distributions). Although an additional 14 GCMs (ACCESS-ESM1-5, BCC-CSM2-MR, CanESM5, EC-Earth3-Veg-LR, FGOALS-g3, GFDL-CM4, GFDL-ESM4, INM-CM4-8, INM-CM5-0, IPSL-CM6A-LR, MIROC6, MPI-ESM1-2-LR, MRI-ESM2-0, and NESM3) satisfy the data availability criterion at the time of retrieving precipitation datasets from the ESGF platform, these models are excluded because their historical or future annual daily precipitation peaks do not pass the K-S test for one or more distribution functions at the 5% significance level. Next, the median values of the recurrence rainfall amounts from the historical GCM simulations are compared with those derived from the station records for each distribution function to quantify the uncertainty introduced by the GCM selection. After testing the ensemble medians against the recurrence rainfall amounts from the station records over the 1950–2014 period for all distribution functions, the same procedure is applied using the best-fitted distribution function (as determined by the K-S test results) for each set of annual daily precipitation peaks. This approach is used to estimate flood discharges suitable for design purposes in practical applications (Yalcin 2024). Finally, to be able to quantify the impact of climate change on the generated synthetic 500-year flood hydrographs of the Hastane Brook basin and its subbasins 1 and 2, the percentage changes in the best-fitted distribution function-based median 500-year recurrence rainfall amounts under the SSP2-4.5 and SSP5-8.5 scenarios are calculated relative to the median value obtained from the CMIP6 historical experiment.

3.2.3. Flood hydrographs under the CMIP6 scenarios

The 500-year recurrence flood hydrographs under the SSP2-4.5 and SSP5-8.5 scenarios are developed for cases with and without the construction of the detention reservoir project. The percentage changes in the median 500-year rainfall amounts under the future scenarios, relative to the median 500-year rainfall amount from the CMIP6 historical experiment, are

incorporated into the flood hydrograph development for the SSP2-4.5 and SSP5-8.5 scenarios. To achieve this, the 500-year flood hydrographs for the Hastane Brook basin, subbasin 1, and subbasin 2 are prepared for each future scenario by multiplying the observation-based 500-year rainfall amount with the percentage change attained using the best-fitted distribution function approach. The computations under the superposed Mockus method are performed without altering any other parameters used in deriving synthetic flood hydrographs from the station records. For clarity, the flood hydrographs computed from the station records are referred to as those derived under the historical climate conditions. In contrast, the flood hydrographs calculated by incorporating the percentage changes in the median 500-year rainfall amounts for the future scenarios are referred to as those derived under the climate conditions of the SSP2-4.5 and SSP5-8.5 scenarios.

Since the design of the proposed detention reservoir project is based on the historical climate conditions, the impact of the detention reservoir is considered in the case of the project's construction by accounting for the outflow hydrograph of the spillway structure under both future scenarios. For each future scenario, the 500-year outflow hydrograph of the spillway is generated by applying reservoir routing to the 500-year recurrence flood hydrograph of subbasin 1, using the volume–elevation curve of the reservoir (Yanmaz 2018). The resulting spillway outflow hydrographs are then combined with the ordinate values of the 500-year flood hydrographs of subbasin 2 to produce flood hydrographs for representing the direct impact on the Kirsehir city center under the climate conditions of the SSP2-4.5 and SSP5-8.5 scenarios, assuming that the detention reservoir project is constructed. Flood routing computations through the main channel between the spillway structure and the basin outlet in subbasin 2 are omitted due to the short channel length of approximately 2.2 km. Additionally, in all cases, the initial reservoir volume is assumed to be equal to the dead storage volume corresponding to the minimum water level, and bottom outlet outflows are not included in the computations due to the difficult-to-determine route and capacity of the transmission channel that will pass through the urban region to divert floodwaters from the bottom outlet to Kilicozu Creek.

3.3. 2D Hydrodynamic modeling through HEC-RAS 6.5

3.3.1. Data processing

The source DSM is modified to account for existing flow-blocking structures, including the Hastane overpass, a pedestrian overpass on the Ankara-Kayseri intercity road, and six road culverts and five wooden bridges spanning Kilicozu Creek. These structures appear as closed barriers in the remotely sensed topographic data, obstructing water flow. Additionally, the flow depths in both the natural and channelized sections of Kilicozu Creek are removed from the base surface model. After identifying the dimensional and locational details of these structures, they are reconstructed without their decks using the source terrain in the RAS Mapper interface of HEC-RAS 6.5 software. Subsequently, the creek's underwater bathymetry is integrated with the terrain using the construction plans of the Kentpark recreation area (Sigal 2012) and terrestrial measurements. Any pixel-sized voids in the resulting DSM caused by terrain alterations are filled using the elevation void fill function in ArcGIS software. The final DSM, presented in Figure 2(a), retains the same raster cell size as the source model.

3.3.2. Model construction

Inundation simulations of the Hastane Brook floodplain for the 500-year recurrence interval flooding events, constructed under both historical and future climate scenarios, are performed using a 2D hydrodynamic model developed with HEC-RAS 6.5 software. HEC-RAS 6.5 is selected for this study owing to its advanced 2D unsteady flow routing capabilities, broad recognition in flood hazard assessment studies, and availability as public-domain software, which strengthens reproducibility relative to commercial alternatives. The modeling process begins by integrating the modified DSM of the floodplain into the RAS Mapper interface. A 2D flow area polygon delineating the flood risk zone boundary is then created in the geometric data editor, as illustrated in Figure 2(b). Subsequently, a computational mesh is generated within the defined boundary using a 5 m $\times$ 5 m point spacing, resulting in 107,159 grid cells with an average size of 25.08 m^2, as shown in Figure 2(b). The selected mesh dimensions are sufficient to capture rapid geometric and flow dynamic variations in this urbanized region. After mesh generation, boundary condition (BC) lines are drawn along the perimeter of the 2D flow area to establish the upstream and downstream limits of the flooding. The upstream BC line is set at the mouth of the Hastane basin, while the downstream BC line is located at the far end of Kilicozu Creek. To account for the flows in Kilicozu Creek within the simulation domain, an additional upstream BC line is introduced at the point where the creek intersects the city, as depicted in Figure 2(b).

The land cover raster of the Hastane Brook floodplain, generated with a 0.1 m cell size by processing the region's orthophoto through the maximum likelihood classification tool in ArcGIS software, is used to categorize land features for

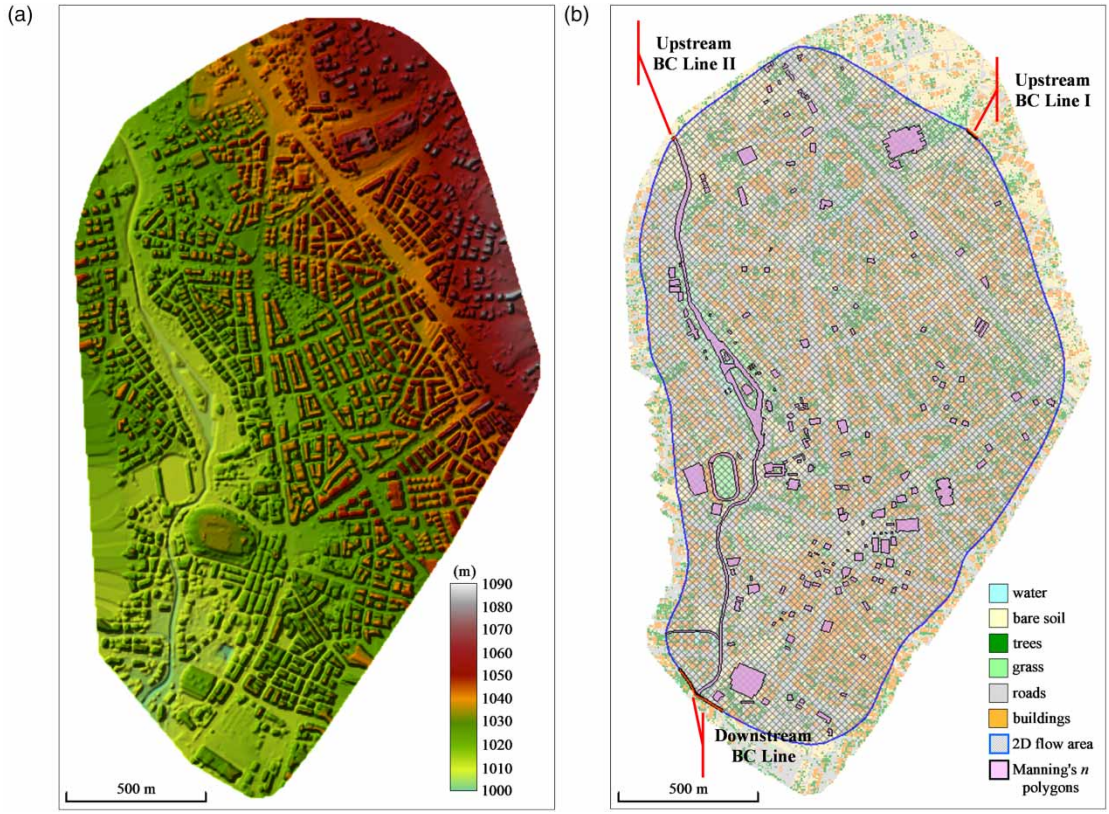

Figure 2 | Terrain and geometric data representation in HEC-RAS 6.5 software for the Hastane Brook floodplain: (a) 4.32 cm cell size DSM modified to account for existing flow-blocking structures and flow depths in Kilicozu Creek and (b) classified land covers, 2D flood area, and upstream/downstream BC lines.

assigning Manning's roughness coefficients. As illustrated in Figure 1, the identified land cover types include water, bare soil, roads, trees, buildings, and grass, though notable misclassifications are evident, particularly for building and water pixels. In developing the hydrodynamic model, the land cover raster is imported into the RAS Mapper interface after being resampled to a 5 m cell size to match the computational grid resolution. Roughness values of 0.02, 0.03, 0.02, 0.06, 10, and 0.035 are assigned to the predefined classes of water, bare soil, roads, trees, buildings, and grass, respectively, within the geometric data editor of HEC-RAS (Chow 1959). For areas affected by misclassification, adjustments to the roughness values are made by defining supplementary Manning's n polygons, as shown in Figure 2(b) (Brunner 2024). Additionally, all water pixels corresponding to the Kilicozu Creek streambed are redefined for glazed tile-lined, concrete-lined with cement rubble masonry sides, and natural creek sections, with roughness coefficients set to 0.015, 0.025, and 0.05, respectively (Chow 1959).

The flow hydrograph- and normal depth-type BCs are configured in the unsteady flow data editor of HEC-RAS to manage inflow and outflow within the simulation domain. For the upstream BC lines, flow hydrographs are used to introduce floodwaters into the 2D flow area. The first upstream BC line, located at the outlet of the Hastane Brook basin, incorporates the 500-year recurrence flood hydrographs generated using 0.5-h Mockus unit hydrographs for both the historical and future climate scenarios, with and without the construction of the detention reservoir project. The flood hydrograph for each scenario is entered at 0.5-h intervals. For the second upstream BC line, a constant baseflow rate of 3.34 m^3/s from Kilicozu Creek is specified for the entire simulation period of each model run. In addition to the flood hydrographs, defining the energy slope is critical for distributing flow along the BC line at each computational time step (Brunner 2024). Energy slopes are assigned values of 0.03 and 0.02 m/m, corresponding to the bed slopes adjacent to the first and second upstream BC lines, respectively. For the downstream normal depth-type BC line, a channel slope of 0.01 m/m along the BC line axis is defined as the friction slope for calculating normal depths using Manning's equation (Brunner 2024).

3.3.3. Hydrodynamic model runs under the historical and future climate scenarios

Prior to conducting model simulations, computation options are defined within the unsteady flow analysis editor of the software. HEC-RAS 6.5 offers the capability to execute 2D unsteady flow routing using three equation sets, which are employed to resolve the flow dynamics across the computational mesh. These include the diffusion wave equations (DWE), the shallow water equations (SWE) employing the Eulerian-Lagrangian Method (SWE-ELM), and a more momentum-conservative SWE solution based on the Eulerian Method (SWE-EM). Although the SWE solvers require smaller computational time steps to maintain stability, resulting in longer simulation runtimes compared with the DWE solver, the SWE-ELM is preferred due to its ability to produce more accurate simulation outcomes (Brunner 2024). The SWE-EM solver is excluded from consideration in this context, as its application is primarily recommended for detailed analyses of variations in water surface elevations and flow velocities around hydraulic structures, piers, abutments, and areas of tight flow contraction and expansion. Additionally, to ensure the numerical stability of the model, the computational time step is set to 0.1 s, in accordance with the Courant–Friedrichs–Lewy condition (Courant *et al.* 1928; Brunner 2024). Simulations are conducted for the 500-year recurrence flooding scenarios, using a model output time interval of 1 min. The results provide spatially distributed outputs, including the extent of inundation, inundation depths, and flow velocities for each flooding scenario.

4. RESULTS AND DISCUSSION

4.1. Projected changes in annual and seasonal precipitation rates

The study evaluates the performance of both raw and bias-corrected historical GCM simulations against measurements from the Kirsehir MS using statistical metrics, including *md*, nRMSE, KGE, and PBIAS, calculated on a monthly basis. Ideal alignment is indicated by an *md* value of 1, an nRMSE value of 0, a KGE value of 1, and a PBIAS value of 0. Accordingly, the raw precipitation simulations exhibit significant variability in error metrics across different CMIP6 models. However, bias correction substantially reduces the magnitude and range of errors. Compared with the measurements from the synoptic MS, the raw GCM outputs under the CMIP6 historical experiment yield *md*, nRMSE, KGE, and PBIAS ranges of 0.52–0.91, 0.06–0.48, 0.41–0.93, and −57.1 to 4.0%, respectively, with median values of 0.69, 0.28, 0.63, and −20.0%. After bias adjustment, these metrics improve significantly, with ranges of 0.90–0.98, 0.02–0.07, 0.93–0.98, and −3.7 to 6.3%, and corresponding medians of 0.97, 0.02, 0.97, and −2.3%.

During the historical period from 1950 to 2014, the observed mean annual precipitation rate is 1.03 mm/day, closely aligning with the bias-corrected CMIP6 model simulations, which yield an ensemble median rate of 1.06 mm/day. This strong concordance extends to seasonal averages. While the mean seasonal observed precipitation rates are 0.84, 1.41, 1.38, and 0.50 mm/day for the autumn, winter, spring, and summer months, the mean seasonal median rates for the GCM simulations are 0.86, 1.46, 1.41, and 0.52 mm/day, respectively. Using the ensemble medians from the CMIP6 historical experiment as a baseline, future changes in mean annual and seasonal precipitation rates at the Kirsehir MS location are analyzed for 2025–2099 under the SSP2-4.5 and SSP5-8.5 scenarios. Accordingly, under SSP2-4.5 and SSP5-8.5, the mean annual daily precipitation is projected to decrease by 1.7 and 7.1%, respectively, compared with the historical median. Seasonally, under SSP2-4.5, the projected changes are −15.4, 4.7, −1.3, and 1.4% for autumn, winter, spring, and summer, respectively. For SSP5-8.5, the corresponding seasonal changes are −16.1, −1.5, −7.4, and −6.9%. Bağçaci *et al.* (2021) examined potential future precipitation anomalies for 2030–2100 across the seven geographical regions of Turkey using ensemble projections of the best-performing CMIP6 GCMs under the SSP2-4.5 and SSP5-8.5 scenarios. The anomalies obtained for the coordinates of the Kirsehir MS in the present study are consistent with their findings for the Central Anatolia Region, which encompasses the Kirsehir MS.

4.2. Projected changes in recurrence rainfall amounts

Before quantifying the effects of climate change on the 500-year flood hydrographs of the Hastane Brook basin and its sub-basins, the performance of the selected 10 GCMs in simulating annual daily precipitation peaks is evaluated. Specifically, the accuracy of the 5-, 10-, 25-, 50-, 100-, and 500-year recurrence rainfall amounts at the Kirsehir MS location under the CMIP6 historical experiment is assessed by comparing these values with those derived from the Kirsehir MS records for the 1950–2014 period. The recurrence rainfall amounts obtained from the bias-corrected historical annual maximum daily precipitation time series for each GCM are presented as box-and-whisker plots in Figure 3(a)–3(d), with their medians listed in Table 3. The rainfall magnitudes calculated from the station records are also included in Figure 3(a)–3(d) and Table 3. Results for each

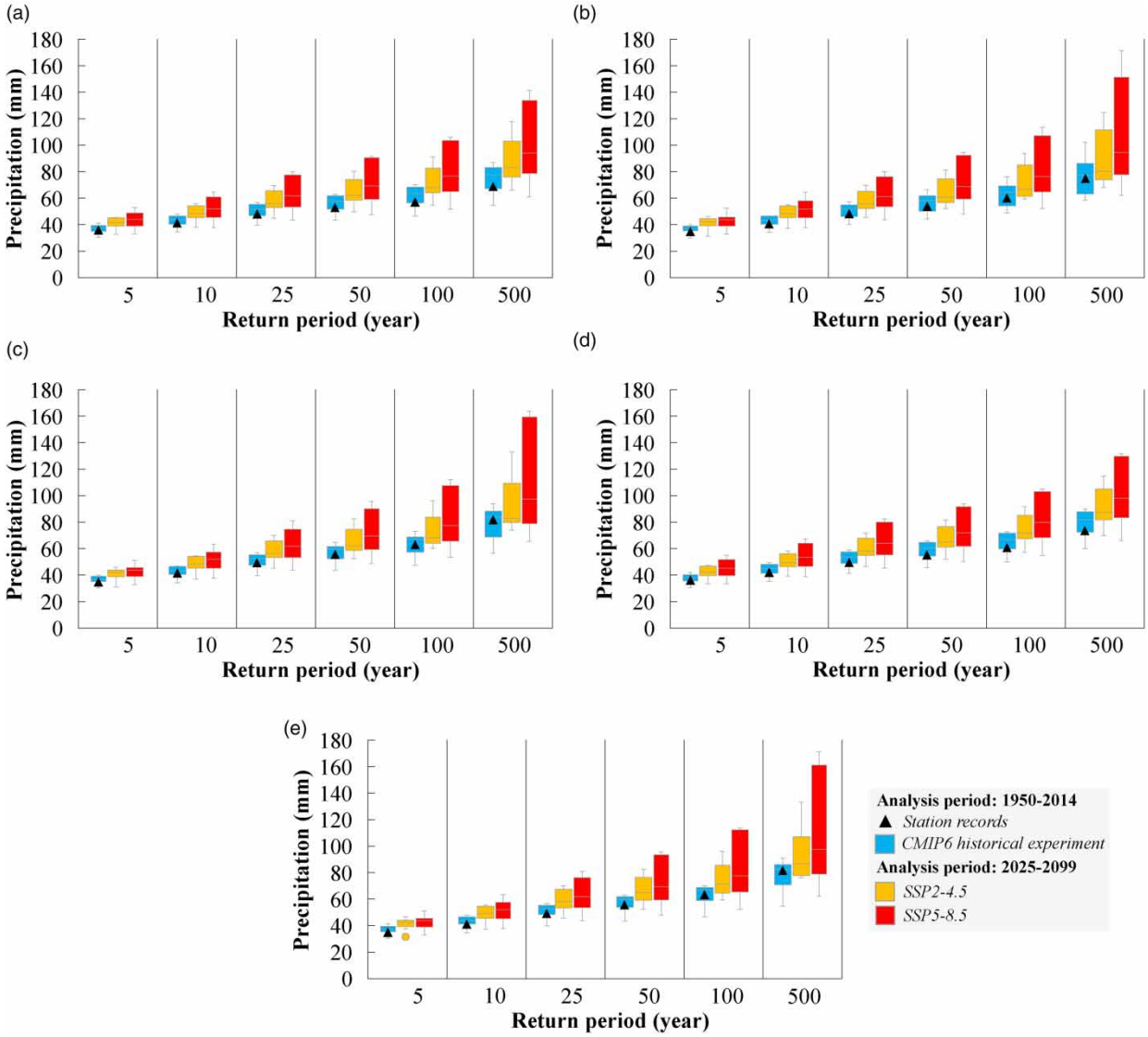

Figure 3 | Recurrence rainfall amounts for the annual maximum daily precipitation projections of the GCMs under the CMIP6 historical experiment and the future societal development scenarios of SSP2-4.5 and SSP5-8.5: (a) log-normal (with two parameters), (b) log-normal (with three parameters), (c) log-Pearson type 3, (d) Gumbel, and (e) best-fitted distribution functions.

distribution function demonstrate a high level of consistency between the median rainfall amounts and the corresponding station-based values. The maximum absolute percentage difference between the ensemble medians and the observation-based amounts is 13.3%, attained for the 500-year return period rainfall magnitude using the log-normal (with two parameters) function. This consistency across all four distribution functions underscores the effectiveness of using medians from a large ensemble to significantly reduce GCM-based uncertainty, particularly for wide ranges of rainfall magnitudes with long return periods, as illustrated in Figure 3(a)–3(d).

The use of results based on the best-fitted distribution functions for calculating median recurrence rainfall amounts is also examined for the historical analysis period of 1950–2014. The results of the K-S test indicate that, among the considered distribution functions, the log-Pearson type 3 distribution is the most appropriate one for the Kirsehir MS records. However, the most appropriate distribution function varies for each set of annual daily precipitation peaks attained from the bias-corrected historical GCM data, as depicted in Table 4. Since the median rainfall amounts differentiate depending on the distribution function used, deriving median values from the best-fitting functions offers a viable approach instead of selecting a single

Table 3 | Medians of the recurrence rainfall amounts for the annual maximum daily precipitation projections of the GCMs under the CMIP6 historical experiment and the future societal development scenarios of SSP2-4.5 and SSP5-8.5, calculated using the log-normal (with two parameters), log-normal (with three parameters), log-Pearson type 3, Gumbel, and best-fitted distribution functions

			Return period (year)					
Distribution function	**Precipitation data**	**Analysis period**	**5**	**10**	**25**	**50**	**100**	**500**
Log-normal (with two parameters)	Station records	1950–2014	35.8	41.1	47.8	52.6	57.3	68.3
	CMIP6 historical experiment	1950–2014	37.2	43.7	51.7	57.7	63.7	77.3
	SSP2-4.5	2025–2099	41.6	48.1	56.1	62.1	68.1	83.0
	SSP5-8.5	2025–2099	44.1	52.0	61.9	69.3	76.7	94.1
Log-normal (with three parameters)	Station records	1950–2014	35.1	40.8	48.4	54.2	60.2	74.8
	CMIP6 historical experiment	1950–2014	37.1	43.5	51.9	58.2	64.5	77.4
	SSP2-4.5	2025–2099	42.2	48.1	55.6	61.0	66.4	80.0
	SSP5-8.5	2025–2099	43.6	51.8	61.2	68.8	76.4	94.6
Log-Pearson type 3	Station records	1950–2014	34.7	40.6	48.7	55.3	62.4	81.2
	CMIP6 historical experiment	1950–2014	36.6	43.4	52.4	59.6	66.9	83.8
	SSP2-4.5	2025–2099	42.1	48.5	56.1	62.2	68.3	82.9
	SSP5-8.5	2025–2099	43.7	52.0	61.9	69.4	77.6	97.5
Gumbel	Station records	1950–2014	36.3	42.3	49.8	55.4	61.0	73.8
	CMIP6 historical experiment	1950–2014	38.1	45.1	53.9	60.4	66.9	81.9
	SSP2-4.5	2025–2099	42.2	49.3	58.3	65.0	71.7	87.1
	SSP5-8.5	2025–2099	45.2	53.5	64.1	72.0	79.8	97.9
Best-fitted distribution functions	Station records (*log-Pearson type 3*)	1950–2014	34.7	40.6	48.7	55.3	62.4	81.2
	CMIP6 historical experiment	1950–2014	37.2	44.0	52.8	59.7	66.9	82.4
	SSP2-4.5	2025–2099	42.2	49.3	58.3	64.9	71.5	86.8
	SSP5-8.5	2025–2099	43.6	52.0	61.9	69.4	77.6	97.5

Table 4 | Best-fitted distribution functions for the annual maximum daily precipitation projections of the GCMs under the CMIP6 historical experiment and the future societal development scenarios of SSP2-4.5 and SSP5-8.5

	Precipitation data		
Model ID	**CMIP6 historical experiment 1950–2014**	**SSP2-4.5 2025–2099**	**SSP5-8.5 2025–2099**
ACCESS-CM2	Log-normal (with two parameters)	Gumbel	Log-Pearson type 3
CMCC-ESM2	Log-Pearson type 3	Log-normal (with three parameters)	Log-Pearson type 3
EC-Earth3	Log-normal (with two parameters)	Log-normal (with two parameters)	Log-normal (with three parameters)
EC-Earth3-CC	Log-normal (with two parameters)	Gumbel	Log-normal (with three parameters)
EC-Earth3-Veg	Gumbel	Log-normal (with two parameters)	Log-Pearson type 3
KIOST-ESM	Log-normal (with two parameters)	Gumbel	Log-Pearson type 3
MPI-ESM1-2-HR	Log-normal (with two parameters)	Log-normal (with three parameters)	Log-normal (with three parameters)
NorESM2-LM	Log-normal (with two parameters)	Gumbel	Log-normal (with three parameters)
NorESM2-MM	Log-Pearson type 3	Log-Pearson type 3	Log-normal (with three parameters)
TaiESM1	Gumbel	Log-normal (with two parameters)	Log-Pearson type 3

distribution function across all sets of GCM simulations (Yalcin 2024). This approach ensures high consistency with the rainfall amounts derived from the station records, as shown in Figure 3(e) and detailed in Table 3. While values of 34.7, 40.6, 48.7, 55.3, 62.4, and 81.2 mm/day are obtained for the 5-, 10-, 25-, 50-, 100-, and 500-year rainfall amounts using the observed precipitation peaks with the log-Pearson type 3 distribution function, the median rainfall amounts derived using the best-fitting functions are 37.2, 44.0, 52.8, 59.7, 66.9, and 82.4 mm/day, respectively.

The recurrence rainfall amounts based on the bias-corrected annual daily peak precipitation rates of each GCM for the 2025–2099 period under the future societal development scenarios SSP2-4.5 and SSP5-8.5 are depicted in Figure 3(a)–3(d). Correspondingly, the median values of these rainfall amounts are summarized in Table 3. The analysis reveals an upward trend across all projected recurrence rainfall amounts, with more pronounced increases observed under the SSP5-8.5 scenario. However, the percentage increases in the median recurrence rainfall amounts with respect to those under the CMIP6 historical experiment vary depending on the probability distribution function used. Consequently, the evaluation focuses on the median results from the best-fitting distribution functions, with the median amounts from the CMIP6 historical experiment serving as the baseline scenario. Table 4 identifies the best-fitting distribution function for each future precipitation peak series, while Figure 3(e) and Table 3 present the corresponding projected recurrence rainfall amounts and their medians. Under the SSP2-4.5 scenario, the median rainfall amounts for the 5-, 10-, 25-, 50-, 100-, and 500-year return periods increase by 13.4, 12.0, 10.4, 8.7, 6.9, and 5.3%, respectively, compared with the baseline CMIP6 historical experiment conditions. In contrast, the SSP5-8.5 scenario projects even greater increases, with percentage rises of 17.2, 18.2, 17.2, 16.2, 16.0, and 18.3% for the same return periods. Tugrul *et al.* (2025) conducted a comprehensive evaluation of future extreme rainfall patterns for 2015–2100 using a CMIP6 multi-model ensemble combined with a high-resolution reference dataset. Applying quantile delta mapping for downscaling and the generalized extreme value (GEV) distribution to estimate 5-, 50-, and 100-year return levels of daily maximum precipitation, they identified spatial patterns of projected changes under the SSP2-4.5 and SSP5-8.5 scenarios. The return levels projected for the Kirsehir station in this study are consistent with their estimates for the corresponding recurrence periods.

4.3. Projected changes in flood hydrographs

The historical 500-year flood hydrograph of the Hastane Brook basin, generated using the superposed Mockus method for the 500-year return period rainfall amount derived from the annual maximum daily precipitation records of the Kirsehir MS with the log-Pearson type 3 distribution function, is presented in Figure 4(a). The 500-year recurrence interval flood hydrographs for the Hastane basin under the future scenarios SSP2-4.5 and SSP5-8.5 are produced by applying a 5.3 and 18.3% increase, respectively, to the observation-based 500-year return period rainfall magnitude. These values correspond to the percentage increases in the median 500-year rainfall amounts under the future societal development scenarios relative to the median 500-year rainfall amount from the CMIP6 historical experiment (Table 3). The future-based 500-year flood hydrographs are included in Figure 4(a), along with their 95% confidence intervals, to illustrate the impact of climate change on the basin's potential for flooding as well as the associated GCM uncertainty. Accordingly, while the peak discharge, time to peak discharge, base time, and flow volume for the historical 500-year flood hydrograph of the basin are 26.7 m^3/s, 2 h, 6 h, and 0.28 hm^3, respectively, the peak discharge and flow volume are projected to increase to 29.2 m^3/s and 0.31 hm^3 for the SSP2-4.5 scenario, and to 36.3 m^3/s and 0.38 hm^3 for the SSP5-8.5 scenario. Moreover, while the base time remains unchanged under both future scenarios, the time to peak discharge decreases to 1.5 h under the SSP5-8.5 scenario, whereas the peak time remains 2 h for the SSP2-4.5 scenario.

For the analysis of the case involving the construction of the detention reservoir project, the 500-year recurrence interval flood hydrographs of the Hastane Brook subbasins are generated for both historical and future climate conditions, as presented in Figure 4(b) and 4(c). The proposed detention reservoir is sized as specified in Table 2, using the observation-based 500-year flood hydrograph of subbasin 1, shown in Figure 4(b). Since no spillway outflow will occur under the 500-year historical flooding scenario, the observation-based 500-year flood hydrograph of subbasin 2, which has a peak discharge rate of 4.7 m^3/s, a peak time of 1 h, a base time of 5 h, and a flow volume of 0.04 hm^3, as depicted in Figure 4(c), is used as input data in the hydrodynamic model run for the historical scenario involving the project's construction. Figure 4(d) presents the outflow hydrographs of the proposed spillway structure, obtained by applying reservoir routing to the 500-year recurrence interval flood hydrographs of subbasin 1 under the climate conditions of the SSP2-4.5 and SSP5-8.5 scenarios, assuming that the initial reservoir volume equals the dead storage volume. The flood hydrographs used as input data for the future SSP2-4.5 and SSP5-8.5 scenarios, in the case of the project's construction, are generated by combining the resulting spillway outflow hydrographs with the ordinate values of the 500-year flood hydrographs of subbasin 2, as shown in Figure 4(e). Accordingly, for the SSP2-4.5 scenario, the peak discharge, time to peak discharge, base time, and flow volume for the 500-year flood hydrograph of the Hastane Brook basin with the detention reservoir project are 5.3 m^3/s, 1 h, 8 h, and 0.07 hm^3, respectively. The corresponding hydrograph characteristics for the SSP5-8.5 scenario are 10.5 m^3/s, 4 h, 8 h, and 0.12 hm^3, respectively.

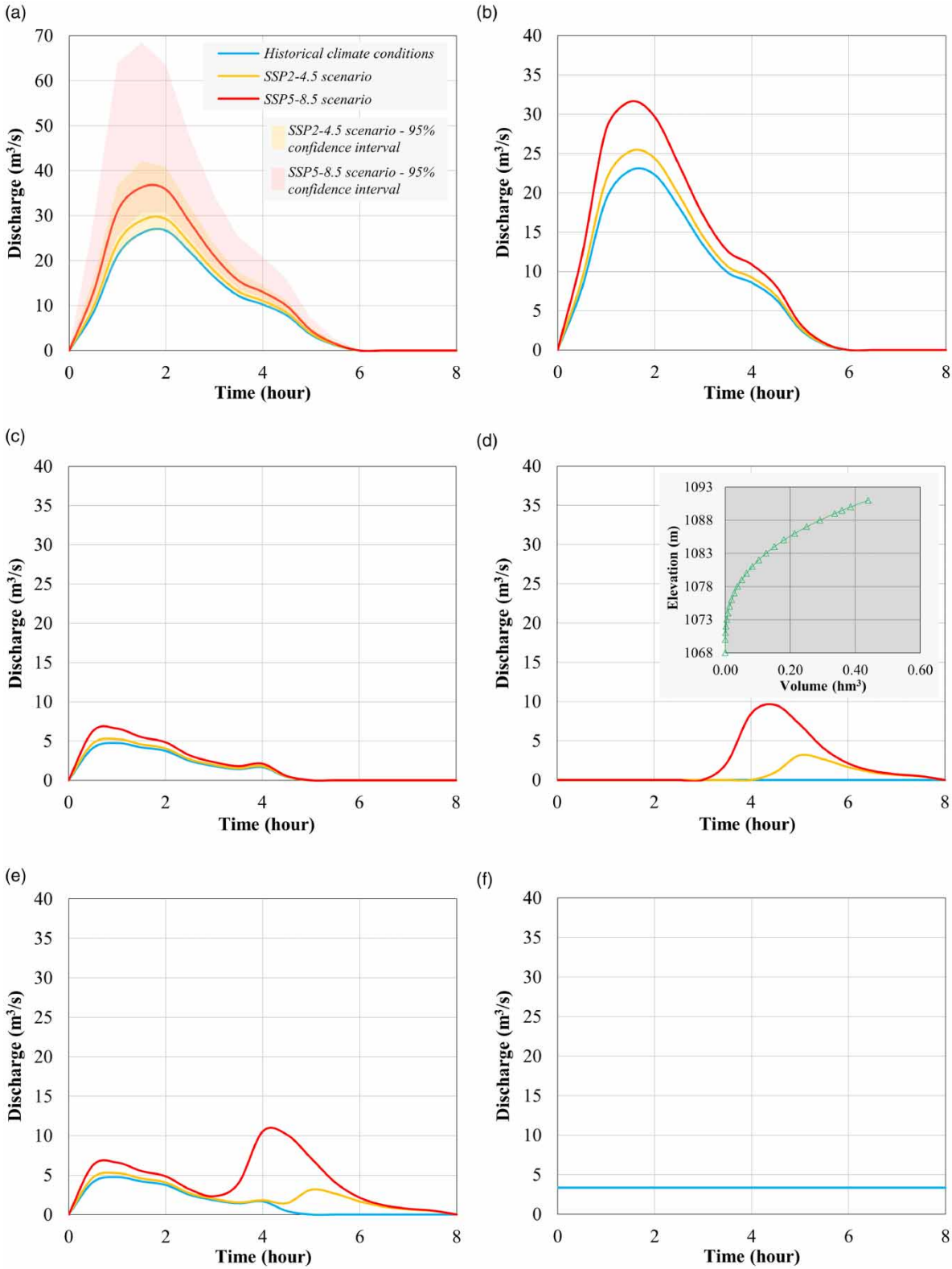

Figure 4 | 500-year flood hydrographs derived under the historical climate conditions, SSP2-4.5 scenario, and SSP5-8.5 scenario for (a) Hastane Brook basin (without the detention reservoir project), (b) subbasin 1, (c) subbasin 2, (d) subbasin I (outflow hydrograph of the detention reservoir), and (e) Hastane Brook basin (after the construction of the detention reservoir), along with (f) baseflow hydrograph of the Kilicozu Creek basin.

4.4. Projected changes in flooding impacts

The developed HEC-RAS model is run six times under 2D hydrodynamic unsteady flow conditions by configuring the first upstream BC with the 500-year recurrence interval flood hydrographs of the Hastane Brook basin, derived for the historical climate conditions, the SSP2-4.5 scenario, and the SSP5-8.5 scenario, for cases both with and without the detention reservoir project, as presented in Figure 4(a) and 4(e). In all model runs, the second upstream BC is configured with the constant-rate baseflow hydrograph of Kilicozu Creek, as shown in Figure 4(f). Accordingly, the inundation depth, flow velocity, and flood danger maps derived for the 500-year flood hydrographs of the Hastane basin under the historical and future climate conditions are presented in Figure 5(a)–5(c) for the case without the detention reservoir project and Figure 6(a)–6(c) for the case with the project. For both cases, the spatial inundation depths and flow velocities represent the maximum cell values obtained from model outputs at 1-min intervals throughout the simulation period. The flood danger maps classify flood risk zones over the Hastane Brook floodplain based on flood intensity ratings calculated for each cell of the 2D computational mesh across the inundation area (de Moel *et al.* 2009). The flood intensity rating of a grid cell is determined using the maximum value of the product of inundation depth and the sum of flow velocity plus 0.5 attained for that cell throughout the simulation period. Intensity levels are classified qualitatively as *extreme* if the maximum value is 2.5 or higher, *significant* if between 1.25 and 2.5, *moderate* if between 0.75 and 1.25, and *low* if 0.75 or lower. These levels correspond to different degrees of risk: low indicates caution, moderate is dangerous for some (e.g., children), significant is dangerous for most people, and extreme is dangerous for all (HR Wallingford *et al.* 2006; Maruti *et al.* 2018). The statistical analysis of the spatial results from the 2D hydrodynamic simulations over the Hastane Brook floodplain is summarized in Table 5.

The model simulation conducted for the historical climate conditions, in the absence of the proposed detention reservoir project, yields a total inundation area of 0.28 km^2, a mean inundation depth of 0.59 m, a mean flow velocity of 0.72 m/s, and a mean flood intensity rating of 1.55 m^2/s. The inundation area is distributed across flood danger classifications as follows: 69.3% *low*, 12.5% *moderate*, 12.5% *significant*, and 5.7% *extreme*, corresponding to regions of 0.20, 0.03, 0.03, and 0.02 km^2, respectively. It is observed that the results for flooding extent, inundation depths, and flow velocities obtained under the historical scenario are highly consistent with those in Yalcin (2019), which were attained using an older version of HEC-RAS (i.e., HEC-RAS 5.0) and a different solver (i.e., full momentum (Saint Venant) equations) for 2D unsteady flood routing. On the other hand, while the flow volumes of the 500-year return period flood hydrographs for the Hastane basin, simulated under the SSP2-4.5 and SSP5-8.5 scenarios, are 9.8 and 34.9% higher than that of the historical 500-year flood hydrograph of the basin, the model simulations under the climate conditions of the SSP2-4.5 and SSP5-8.5 scenarios expand the inundation area by 5.1 and 15.9%, respectively. The increases in mean inundation depth for the SSP2-4.5 and SSP5-8.5 scenarios, relative to the mean inundation depth under the historical climate conditions, are quantified as 2.0 and 8.4%, respectively. However, neither future scenario shows a noteworthy increase in flow velocity or flood intensity rating averages. Nevertheless, the inundated area classified as *moderate*, *significant*, or *extreme* increases by 7.3 and 24.7% under the SSP2-4.5 and SSP5-8.5 scenarios, respectively, compared with the historical climate scenario.

The proposed detention reservoir, characterized by an active storage capacity of approximately 0.24 hm^3, mitigates the flow volume of the historical 500-year flood hydrograph of the Hastane Brook basin, reducing it to 0.04 hm^3. With the detention reservoir in place, a 500-year flood event under the historical climate conditions results in an inundation area of 0.16 km^2, a mean inundation depth of 0.37 m, a mean flow velocity of 0.51 m/s, and a mean flood intensity rating of 1.14 m^2/s. Under these conditions, the post-construction distribution of flood hazard classifications within the inundation zone is as follows: 88.2% *low*, 9.5% *moderate*, 2.0% *significant*, and 0.3% *extreme*. Despite a 52.4% increase in the 500-year flood hydrograph volume under the SSP2-4.5 scenario relative to the historical climate scenario with the reservoir project, flood characteristics, including extent, mean inundation depth, mean flow velocity, and spatial distribution of flood danger zones, remain largely unchanged. However, under the SSP5-8.5 scenario, the projected impacts of a 500-year flood event indicate that the efficacy of the detention reservoir, designed for the historical climate conditions, will be partially diminished due to the increase in the 500-year flood hydrograph volume from 0.04 to 0.12 hm^3 in this high-forcing future scenario. The model simulation performed under the SSP5-8.5 climate conditions results in an inundation area of 0.20 km^2, a mean inundation depth of 0.46 m, a mean flow velocity of 0.62 m/s, and a mean flood intensity rating of 1.31 m^2/s. These values represent increases of 26.4, 26.0, 20.4, and 14.9%, respectively, relative to the historical scenario. Moreover, the inundated area classified as *moderate*, *significant*, or *extreme* in the flood danger map for the SSP5-8.5 scenario is 145.3% larger than in the historical climate

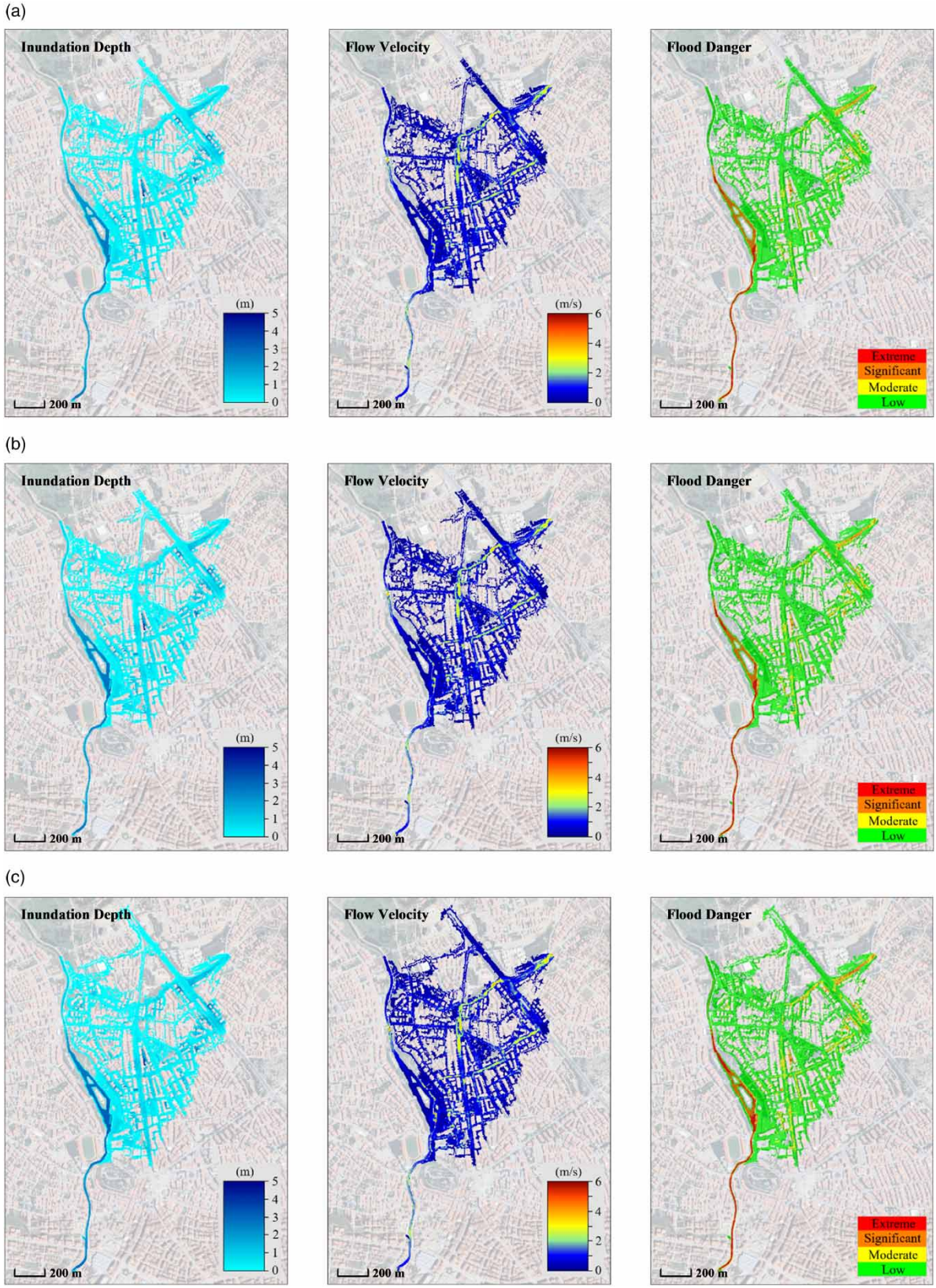

Figure 5 | 500-year recurrence interval inundation depth, flow velocity, and flood danger maps of the Hastane Brook floodplain without the detention reservoir project under (a) historical climate conditions, (b) SSP2-4.5 scenario, and (c) SSP5-8.5 scenario.

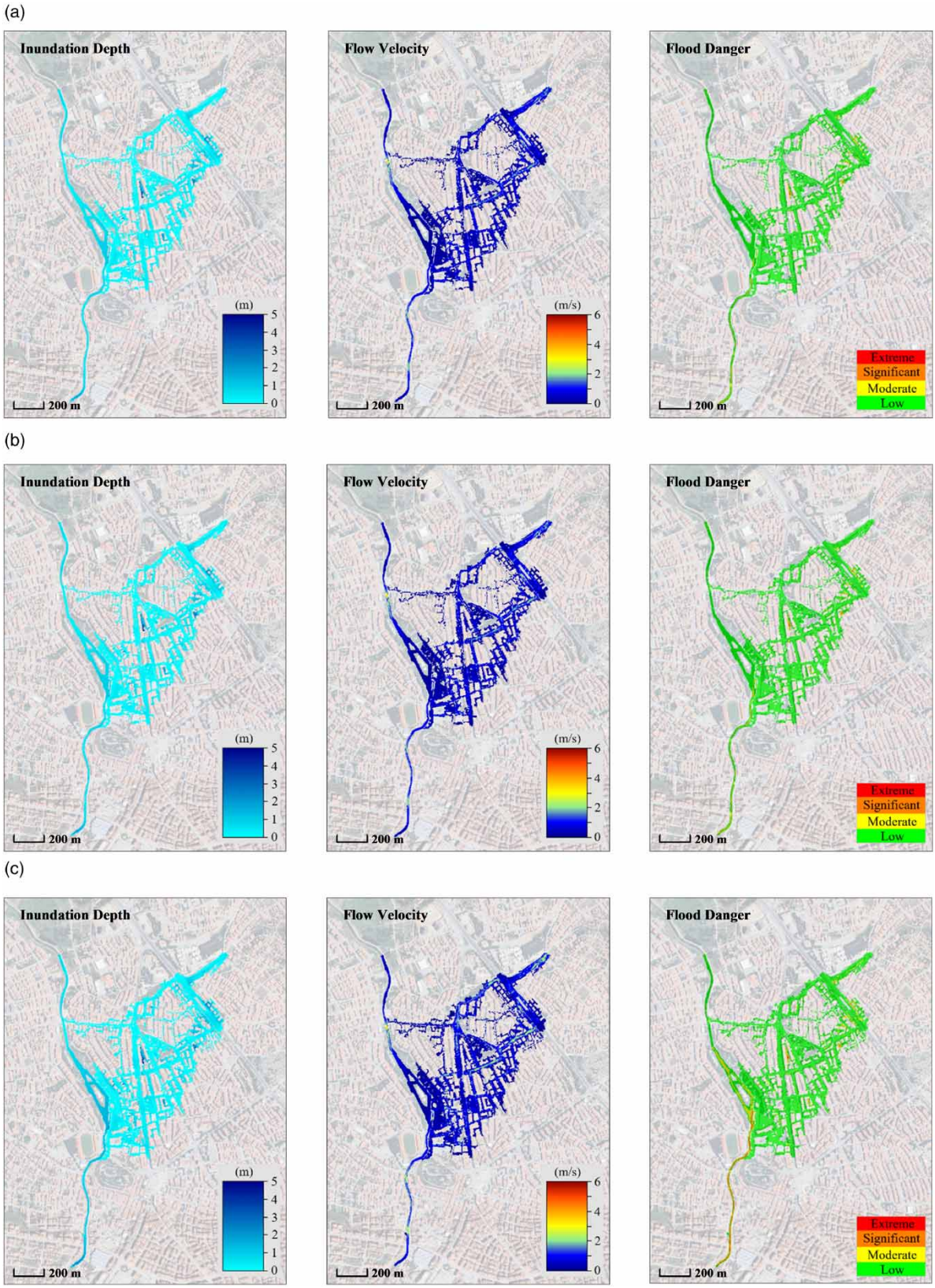

Figure 6 | 500-year recurrence interval inundation depth, flow velocity, and flood danger maps of the Hastane Brook floodplain after the construction of the detention reservoir under (a) historical climate conditions, (b) SSP2-4.5 scenario, and (c) SSP5-8.5 scenario.

Table 5 | Statistical analysis of the spatial results from the 2D hydrodynamic simulations over the Hastane Brook floodplain, considering both the absence and presence of the detention reservoir

Simulation statistics			Without the detention reservoir			With the detention reservoir		
			Historical climate conditions	SSP2-4.5 scenario	SSP5-8.5 scenario	Historical climate conditions	SSP2-4.5 scenario	SSP5-8.5 scenario
Inundation area		km^2	0.28	0.29	0.32	0.16	0.16	0.20
Inundation depth, D	Max	m	4.72	4.75	4.79	4.41	4.43	4.56
	Mean	m	0.59	0.61	0.64	0.37	0.37	0.46
	Standard deviation	m	0.68	0.70	0.78	0.38	0.39	0.46
Flow velocity, V	Max	m/s	5.04	5.26	5.76	3.94	3.94	3.95
	Mean	m/s	0.72	0.72	0.74	0.51	0.52	0.62
	Standard deviation	m/s	0.65	0.66	0.68	0.44	0.45	0.53
Flood danger, FD $FD = D \times (V + 0.5)$	FD: Low (1)	%	69.3	68.7	67.0	88.2	87.5	77.1
	FD: Moderate (2)	%	12.5	12.9	13.6	9.5	10.0	14.8
	FD: Significant (3)	%	12.5	12.3	11.7	2.0	2.2	7.7
	FD: Extreme (4)	%	5.7	6.1	7.7	0.3	0.3	0.4
	Mean	m^2/s	1.55	1.56	1.60	1.14	1.15	1.31
	Standard deviation	m^2/s	0.92	0.93	0.97	0.43	0.44	0.63

scenario with the detention reservoir project, while being 45.7% smaller than in the historical scenario without the reservoir project.

When the dimensions of the proposed project are reevaluated, considering the 500-year return period flood hydrograph of subbasin 1 produced for the climate conditions of the SSP5-8.5 scenario, it becomes evident that increasing the dam crest elevation, originally designed at 23 m above the thalweg, by just 1.5 m would be sufficient to accommodate the required reservoir volume. Accordingly, with the dam crest raised by 1.5 m, a model simulation, performed by configuring the first upstream BC with the 500-year flood hydrograph of subbasin 2 for the SSP5-8.5 scenario, produces flood statistics that closely match those from the historical scenario with the original project design, as presented in Figure 7. Under the revised embankment

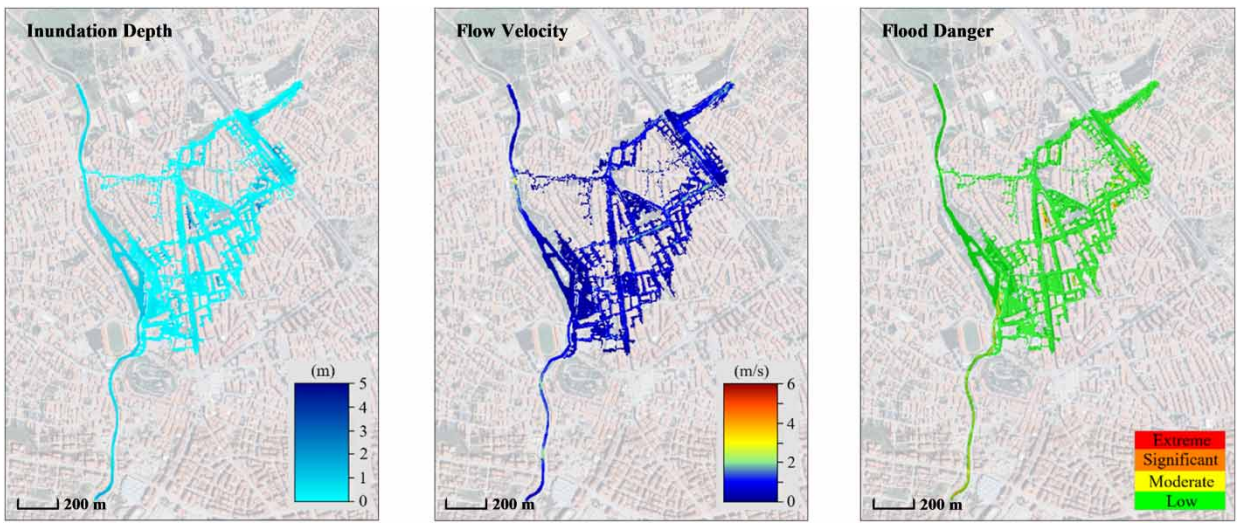

Figure 7 | 500-year recurrence interval inundation depth, flow velocity, and flood danger maps of the Hastane Brook floodplain after the construction of a higher capacity detention reservoir dimensioned for the SSP5-8.5 scenario.

design, the impact of a 500-year flooding event on the floodplain under the SSP5-8.5 scenario results in an inundation area of 0.17 km^2, a mean inundation depth of 0.39 m, a mean flow velocity of 0.56 m/s, and a mean flood intensity rating of 1.17 m^2/s. The resulting distribution of flood danger classifications within the inundation zone is as follows: 86.2% *low*, 10.6% *moderate*, 2.9% *significant*, and 0.3% *extreme*. Thus, it can be concluded that integrating climate change projections such as SSP5-8.5 into flood mitigation infrastructure design is advisable. However, additional factors must also guide decision-making. These include the project's strategic importance, economic feasibility, projected lifespan, and associated risks to economic stability and human safety. Selecting appropriate climate scenarios for long-term planning requires a balanced approach that accounts for both future uncertainties and practical considerations.

5. CONCLUSIONS

This study proposes an integrated framework to quantify the adequacy of a detention reservoir designed using historical precipitation data, assuming climate change follows either the medium-forcing SSP2-4.5 or high-forcing SSP5-8.5 scenario. The focus is on the Hastane Brook basin and its urban floodplain in Kirsehir Province, Turkey. The hydrodynamic model simulation, conducted using the basin's historical-based flood hydrograph without considering the proposed detention reservoir, highlights the urgent need for a flood mitigation structure. This need becomes even more critical under both future scenarios. While the model simulations incorporating the detention reservoir indicate that flooding characteristics remain largely unchanged under the SSP2-4.5 scenario, they reveal that the reservoir capacity will be insufficient to accommodate the projected flood hydrograph volume if climate change follows the SSP5-8.5 scenario. Although several studies have shown that higher-resolution DSMs produce more accurate flood hazard maps than coarser-resolution DSMs, which often lead to overestimation of inundation extents, relying solely on a high-resolution DSM with centimeter-scale localization accuracy does not guarantee reliable model outputs (Marks & Bates 2000; Omer *et al.* 2003; Cook & Merwade 2009; Saksena & Merwade 2015). However, verifying the simulation outputs is not possible for this case due to the lack of historical flood records and the evolving topography of the floodplain over time (Yalcin 2019). Therefore, rather than analyzing the simulation results on a point-by-point basis across the urban floodplain, the study discusses changes in general flooding characteristics based on mean values.

The proposed methodology is expected to support the design of flood control structures in basins where climate change is likely to pose a significant threat to water resources in the coming decades. For future studies, it is advisable to assess the impact of climate change on flood hydrographs not only by using synthetic unit hydrograph methods but also by incorporating statistical approaches based on streamflow projections (Yalcin 2024). For such an analysis, when simulating streamflow through hydrological models, the proposed framework can be extended to include future variations in other climatic variables, such as temperature, wind speed, relative humidity, and solar radiation (Gorguner & Kavvas 2020). Additionally, applying different bias correction techniques and integrating a larger ensemble of GCMs can improve the reliability of rainfall and streamflow projections, making them more consistent with *in-situ* measurements (Wang *et al.* 2020). Furthermore, for point-by-point change assessments on flood hazard maps, calibrating 2D hydrodynamic models with inundation data from at least two past flood events is essential. This calibration process helps address uncertainties related to flood hydrographs, modeling parameters, modeling techniques, and geospatial operations (Merwade *et al.* 2008). Finally, future evaluations of climate change impacts should rely on simulations from CMIP6-based RCMs, which are expected to become increasingly available in the coming years.

DATA AVAILABILITY STATEMENT

All relevant data are included in the paper or its Supplementary Information.

CONFLICT OF INTEREST

The authors declare there is no conflict.

REFERENCES

Abdi-Dehkordi, M., Bozorg-Haddad, O., Salavitabar, A., Mohammad-Azari, S. & Goharian, E. (2021) Development of flood mitigation strategies toward sustainable development, *Natural Hazards*, **108**, 2543–2567. https://doi.org/10.1007/s11069-021-04788-5.

Alfieri, L., Dottori, F., Betts, R., Salamon, P. & Feyen, L. (2018) Multi-model projections of river flood risk in Europe under global warming, *Climate*, **6** (1), 6. https://doi.org/10.3390/cli6010006.

Almeida, M. P., Perpiñán, O. & Narvarte, L. (2015) PV power forecast using a nonparametric PV model, *Solar Energy*, **115**, 354–368. https://doi.org/10.1016/j.solener.2015.03.006.

Arnone, E., Pumo, D., Francipane, A., La Loggia, G. & Noto, L. V. (2018) The role of urban growth, climate change, and their interplay in altering runoff extremes, *Hydrological Processes*, **32** (12), 1755–1770. https://doi.org/10.1002/hyp.13141.

Bağçaci, S. Ç., Yucel, I., Duzenli, E. & Yilmaz, M. T. (2021) Intercomparison of the expected change in the temperature and the precipitation retrieved from CMIP6 and CMIP5 climate projections: a Mediterranean hot spot case, Turkey, *Atmospheric Research*, **256**, 105576. https://doi.org/10.1016/j.atmosres.2021.105576.

Bhusal, A., Thakur, B., Kalra, A., Benjankar, R. & Shrestha, A. (2024) Evaluating the effectiveness of best management practices in adapting the impacts of climate change-induced urban flooding, *Atmosphere*, **15** (3), 281. https://doi.org/10.3390/atmos15030281.

Brunner, G. W. (2024) *HEC-RAS River Analysis System: HEC-RAS 2D Modeling User's Manual (Version 6.5)*. Davis: U.S. Army Corps of Engineers – Hydraulic Engineering Center of the Institute for Water Resources.

Cannon, A. J. (2018) Multivariate quantile mapping bias correction: an *N*-dimensional probability density function transform for climate model simulations of multiple variables, *Climate Dynamics*, **50**, 31–49. https://doi.org/10.1007/s00382-017-3580-6.

Cannon, A. J., Sobie, S. R. & Murdock, T. Q. (2015) Bias correction of GCM precipitation by quantile mapping: how well do methods preserve changes in quantiles and extremes? *Journal of Climate*, **28** (17), 6938–6959. https://doi.org/10.1175/JCLI-D-14-00754.1.

Chow, V. T. (1959) *Open Channel Hydraulics*. New York: McGraw-Hill.

Cook, A. & Merwade, V. (2009) Effect of topographic data, geometric configuration and modeling approach on flood inundation mapping, *Journal of Hydrology*, **377** (1–2), 131–142. https://doi.org/10.1016/j.jhydrol.2009.08.015.

Courant, R., Friedrichs, K. & Lewy, H. (1928) Über die partiellen differenzengleichungen der mathematischen physik [On the partial difference equations of mathematical physics], *Mathematische Annalen*, **100**, 32–74. https://doi.org/10.1007/BF01448839.

de Moel, H., van Alphen, J. & Aerts, J. C. J. H. (2009) Flood maps in Europe – methods, availability and use, *Natural Hazards and Earth System Sciences*, **9** (2), 289–301. https://doi.org/10.5194/nhess-9-289-2009.

Dernek, E. (2012) *Design of Overflow Structures and Example of Kayi River. MSc thesis*. Namik Kemal University.

Dottori, F., Szewczyk, W., Ciscar, J.-C., Zhao, F., Alfieri, L., Hirabayashi, Y., Bianchi, A., Mongelli, I., Frieler, K., Betts, R. A. & Feyen, L. (2018) Increased human and economic losses from river flooding with anthropogenic warming, *Nature Climate Change*, **8**, 781–786. https://doi.org/10.1038/s41558-018-0257-z.

DSI (General Directorate of State Hydraulic Works) (1989) *Preliminary Investigation Report on the Flood Protection Strategy of the Kirsehir City Center*. Kayseri: XIIth Regional Directorate of State Hydraulic Works.

Eren, M. E. (2011) *Investigations on the Flood Risk of the Bogluca (Kayali) Stream. MSc thesis*. Yildiz Technical University.

ESGF (Earth System Grid Federation) (2022) *WCRP Coupled Model Intercomparison Project (Phase 6)*. Available at: https://esgf-node.llnl.gov/projects/cmip6/ [Accessed 15th May 2022].

Gorguner, M. & Kavvas, M. L. (2020) Modeling impacts of future climate change on reservoir storages and irrigation water demands in a Mediterranean basin, *Science of the Total Environment*, **748**, 141246. https://doi.org/10.1016/j.scitotenv.2020.141246.

Gupta, H. V., Kling, H., Yilmaz, K. K. & Martinez, G. F. (2009) Decomposition of the mean squared error and NSE performance criteria: implications for improving hydrological modelling, *Journal of Hydrology*, **377** (1–2), 80–91. https://doi.org/10.1016/j.jhydrol.2009.08.003.

Hirabayashi, Y., Mahendran, R., Koirala, S., Konoshima, L., Yamazaki, D., Watanabe, S., Kim, H. & Kanae, S. (2013) Global flood risk under climate change, *Nature Climate Change*, **3**, 816–821. https://doi.org/10.1038/nclimate1911.

Hosseinzadehtalaei, P., Tabari, H. & Willems, P. (2017) Uncertainty assessment for climate change impact on intense precipitation: how many model runs do we need? *International Journal of Climatology*, **37** (S1), 1105–1117. https://doi.org/10.1002/joc.5069.

HR Wallingford, Middlesex University – Flood Hazard Research Centre, Risk and Policy Analysts Ltd (2006) *Flood Risks to People: Phase 2 - FD2321/TR2 Guidance Document*. London: Department for Environment – Food and Rural Affairs (DEFRA) and Environmental Agency.

Huong, H. T. L. & Pathirana, A. (2013) Urbanization and climate change impacts on future urban flooding in Can Tho city, Vietnam, *Hydrology and Earth System Sciences*, **17** (1), 379–394. https://doi.org/10.5194/hess-17-379-2013.

Jamrussri, S. & Toda, Y. (2017) Simulating past severe flood events to evaluate the effectiveness of nonstructural flood countermeasures in the upper Chao Phraya River Basin, Thailand, *Journal of Hydrology: Regional Studies*, **10**, 82–94. https://doi.org/10.1016/j.ejrh.2017.02.001.

Jiang, Y., Zevenbergen, C. & Ma, Y. (2018) Urban pluvial flooding and stormwater management: a contemporary review of China's challenges and "sponge cities" strategy, *Environmental Science and Policy*, **80**, 132–143. https://doi.org/10.1016/j.envsci.2017.11.016.

Jones, P. W. (1999) First- and second-order conservative remapping schemes for grids in spherical coordinates, *Monthly Weather Review*, **127** (9), 2204–2210. https://doi.org/10.1175/1520-0493(1999)127<2204:FASOCR>2.0.CO;2.

Jongman, B. (2018) Effective adaptation to rising flood risk, *Nature Communications*, **9**, 1986. https://doi.org/10.1038/s41467-018-04396-1.

Jongman, B., Ward, P. J. & Aerts, J. C. J. H. (2012) Global exposure to river and coastal flooding: long term trends and changes, *Global Environmental Change*, **22** (4), 823–835. https://doi.org/10.1016/j.gloenvcha.2012.07.004.

Jongman, B., Winsemius, H. C., Aerts, J. C. J. H., de Perez, E. C., van Aalst, M. K., Kron, W. & Ward, P. J. (2015) Declining vulnerability to river floods and the global benefits of adaptation, *Proceedings of the National Academy of Sciences*, **112** (18), E2271–E2280. https://doi.org/10.1073/pnas.1414439112.

Kaczmarska, J., Jewson, S. & Bellone, E. (2018) Quantifying the sources of simulation uncertainty in natural catastrophe models, *Stochastic Environmental Research and Risk Assessment*, **32**, 591–605. https://doi.org/10.1007/s00477-017-1393-0.

Karamouz, M., Noori, N., Moridi, A. & Ahmadi, A. (2011) Evaluation of floodplain variability considering impacts of climate change, *Hydrological Processes*, **25** (1), 90–103. https://doi.org/10.1002/hyp.7822.

Kinoshita, Y., Tanoue, M., Watanabe, S. & Hirabayashi, Y. (2018) Quantifying the effect of autonomous adaptation to global river flood projections: application to future flood risk assessments, *Environmental Research Letters*, **13**, 014006. https://doi.org/10.1088/1748-9326/aa9401.

Knutti, R., Furrer, R., Tebaldi, C., Cermak, J. & Meehl, G. A. (2010) Challenges in combining projections from multiple climate models, *Journal of Climate*, **23** (10), 2739–2758. https://doi.org/10.1175/2009JCLI3361.1.

Kundzewicz, Z. W. & Stakhiv, E. Z. (2010) Are climate models "ready for prime time" in water resources management applications, or is more research needed? *Hydrological Sciences Journal*, **55** (7), 1085–1089. https://doi.org/10.1080/02626667.2010.513211.

Lawler, J. J. (2009) Climate change adaptation strategies for resource management and conservation planning, *Annals of the New York Academy of Sciences*, **1162** (1), 79–98. https://doi.org/10.1111/j.1749-6632.2009.04147.x.

Legates, D. R. & McCabe, G. J. (1999) Evaluating the use of "goodness-of-fit" measures in hydrologic and hydroclimatic model validation, *Water Resources Research*, **35** (1), 233–241. https://doi.org/10.1029/1998WR900018.

Lehner, F., Wood, A. W., Vano, J. A., Lawrence, D. M., Clark, M. P. & Mankin, J. S. (2019) The potential to reduce uncertainty in regional runoff projections from climate models, *Nature Climate Change*, **9**, 926–933. https://doi.org/10.1038/s41558-019-0639-x.

Mahmoud, S. H. & Gan, T. Y. (2018) Urbanization and climate change implications in flood risk management: developing an efficient decision support system for flood susceptibility mapping, *Science of the Total Environment*, **636**, 152–167. https://doi.org/10.1016/j.scitotenv.2018.04.282.

Mahmood, M. I., Elagib, N. A., Horn, F. & Saad, S. A. G. (2017) Lessons learned from Khartoum flash flood impacts: an integrated assessment, *Science of the Total Environment*, **601–602**, 1031–1045. https://doi.org/10.1016/j.scitotenv.2017.05.260.

Marks, K. & Bates, P. (2000) Integration of high-resolution topographic data with floodplain flow models, *Hydrological Processes*, **14** (11–12), 2109–2122. https://doi.org/10.1002/1099-1085(20000815/30)14:11/12<2109::AID-HYP58 > 3.0.CO;2-1.

Maruti, S. F., Amerudin, S., Kadir, W. H. W. & Yusof, Z. M. (2018) A hydrodynamic modelling of proposed dams in reducing flood hazard in Kelantan Catchment, *IOP Conference Series: Earth and Environmental Science*, **140**, 012043. https://doi.org/10.1088/1755-1315/140/1/012043.

Mateus, C. & Tullos, D. (2017) Reliability, sensitivity, and uncertainty of reservoir performance under climate variability in basins with different hydrogeologic settings in Northwestern United States, *International Journal of River Basin Management*, **15** (1), 21–37. https://doi.org/10.1080/15715124.2016.1247361.

McCuen, R. H. (1993) *Microcomputer Applications in Statistical Hydrology*. New Jersey: Prentice Hall.

Merwade, V., Olivera, F., Arabi, M. & Edleman, S. (2008) Uncertainty in flood inundation mapping: current issues and future directions, *Journal of Hydrologic Engineering*, **13** (7), 608–620. https://doi.org/10.1061/(ASCE)1084-0699(2008)13:7(608).

MGM (Turkish State Meteorological Service) (2024a) *Annual Maximum Precipitation Records in Standard Times for the Kirsehir Meteorological Station (Station ID: 17160)*. Ankara: Turkish State Meteorological Service.

MGM (Turkish State Meteorological Service) (2024b) *Daily Precipitation Records of the Kirsehir Meteorological Station (Station ID: 17160)*. Ankara: Turkish State Meteorological Service.

MGM (Turkish State Meteorological Service) (2024c) *Long-Term All Parameters Bulletin for the Kirsehir Meteorological Station (Station ID: 17160)*. Ankara: Turkish State Meteorological Service.

MGM (Turkish State Meteorological Service) (2024d) *Long-Term All Parameters Bulletin for the Kaman Meteorological Station (Station ID: 17756)*. Ankara: Turkish State Meteorological Service.

Mileti, D. S. & Gailus, J. L. (2005) Sustainable development and hazards mitigation in the United States: disasters by design revisited, *Mitigation and Adaptation Strategies for Global Change*, **10**, 491–504. https://doi.org/10.1007/s11027-005-0057-4.

Murphy, J. M., Sexton, D. M. H., Barnett, D. N., Jones, G. S., Webb, M. J., Collins, M. & Stainforth, D. A. (2004) Quantification of modelling uncertainties in a large ensemble of climate change simulations, *Nature*, **430**, 768–772. https://doi.org/10.1038/nature02771.

Omer, C. R., Nelson, E. J. & Zundel, A. K. (2003) Impact of varied data resolution on hydraulic modeling and floodplain delineation, *Journal of the American Water Resources Association*, **39** (2), 467–475. https://doi.org/10.1111/j.1752-1688.2003.tb04399.x.

O'Neill, B. C., Tebaldi, C., van Vuuren, D. P., Eyring, V., Friedlingstein, P., Hurtt, G., Knutti, R., Kriegler, E., Lamarque, J.-F., Lowe, J., Meehl, G. A., Moss, R., Riahi, K. & Sanderson, B. M. (2016) The Scenario Model Intercomparison Project (ScenarioMIP) for CMIP6, *Geoscientific Model Development*, **9** (9), 3461–3482. https://doi.org/10.5194/gmd-9-3461-2016.

Ozdemir, H. (1978) *Applied Flood Hydrology*. Ankara: General Directorate of State Hydraulic Works.

Pathak, S., Liu, M., Jato-Espino, D. & Zevenbergen, C. (2020) Social, economic and environmental assessment of urban sub-catchment flood risks using a multi-criteria approach: a case study in Mumbai city, India, *Journal of Hydrology*, **591**, 125216. https://doi.org/10.1016/j.jhydrol.2020.125216.

Ponce, V. M. & Hawkins, R. H. (1996) Runoff curve number: has it reached maturity? *Journal of Hydrologic Engineering*, **1** (1), 11–19. https://doi.org/10.1061/(ASCE)1084-0699(1996)1:1(11).

Prudhomme, C., Wilby, R. L., Crooks, S., Kay, A. L. & Reynard, N. S. (2010) Scenario-neutral approach to climate change impact studies: application to flood risk, *Journal of Hydrology*, **390** (3–4), 198–209. https://doi.org/10.1016/j.jhydrol.2010.06.043.

Rathjens, H., Bieger, K., Srinivasan, R., Chaubey, I. & Arnold, J. G. (2016) *CMhyd User Manual: Documentation for Preparing Simulated Climate Change Data for Hydrologic Impact Studies*. Available at: https://swat.tamu.edu/media/115265/bias_cor_man.pdf [Accessed 25th May 2022].

Rosbjerg, D. (2017) Optimal adaptation to extreme rainfalls in current and future climate, *Water Resources Research*, **53** (1), 535–543. https://doi.org/10.1002/2016WR019718.

Saksena, S. & Merwade, V. (2015) Incorporating the effect of DEM resolution and accuracy for improved flood inundation mapping, *Journal of Hydrology*, **530**, 180–194. https://doi.org/10.1016/j.jhydrol.2015.09.069.

Salman, S. A., Nashwan, M. S., Ismail, T. & Shahid, S. (2020) Selection of CMIP5 general circulation model outputs of precipitation for peninsular Malaysia, *Hydrology Research*, **51** (4), 781–798. https://doi.org/10.2166/nh.2020.154.

Schoppa, L., Barendrecht, M. H., Paprotny, D., Sairam, N., Sieg, T. & Kreibich, H. (2024) Projecting flood risk dynamics for effective long-term adaptation, *Earth's Future*, **12** (3), e2022EF003258. https://doi.org/10.1029/2022EF003258.

Shiogama, H., Stone, D., Emori, S., Takahashi, K., Mori, S., Maeda, A., Ishizaki, Y. & Allen, M. R. (2016) Predicting future uncertainty constraints on global warming projections, *Scientific Reports*, **6**, 18903. https://doi.org/10.1038/srep18903.

Sigal (Sigal Engineering Trade and Industry Limited Company) (2012) *Description Report on the Infrastructure Projects of the Kirsehir Kilicozu Creek Recreation Area*. Ankara: Sigal Engineering Trade and Industry Limited Company.

Skougaard Kaspersen, P., Ravn, N. H., Arnbjerg-Nielsen, K., Madsen, H. & Drews, M. (2017) Comparison of the impacts of urban development and climate change on exposing European cities to pluvial flooding, *Hydrology and Earth System Sciences*, **21** (8), 4131–4147. https://doi.org/10.5194/hess-21-4131-2017.

SYGM (General Directorate of Water Management) (2019) *Flood Management Plan of the Kizilirmak Basin*. Ankara: General Directorate of Water Management.

Tan, M. L., Juneng, L., Tangang, F. T., Samat, N., Chan, N. W., Yusop, Z. & Ngai, S. T. (2020) Southeast Asia hydrO-meteorological droughT (SEA-HOT) framework: a case study in the Kelantan River Basin, Malaysia, *Atmospheric Research*, **246**, 105155. https://doi.org/10.1016/j.atmosres.2020.105155.

Tanoue, M., Hirabayashi, Y. & Ikeuchi, H. (2016) Global-scale river flood vulnerability in the last 50 years, *Scientific Reports*, **6**, 36021. https://doi.org/10.1038/srep36021.

Teutschbein, C. & Seibert, J. (2012) Bias correction of regional climate model simulations for hydrological climate-change impact studies: review and evaluation of different methods, *Journal of Hydrology*, **456–457**, 12–29. https://doi.org/10.1016/j.jhydrol.2012.05.052.

Tugrul, T., Oruc, S. & Gunes, B. (2025) Quantifying future rainfall extremes in Türkiye: a CMIP6 ensemble approach with statistical downscaling, *Acta Geophysica*, **73**, 3477–3494. https://doi.org/10.1007/s11600-025-01551-3.

Usul, N. (2009) *Engineering Hydrology*. Ankara: METU Press.

van Roosmalen, L., Christensen, J. H., Butts, M. B., Jensen, K. H. & Refsgaard, J. C. (2010) An intercomparison of regional climate model data for hydrological impact studies in Denmark, *Journal of Hydrology*, **380** (3–4), 406–419. https://doi.org/10.1016/j.jhydrol.2009.11.014.

Wang, L. & Chen, W. (2014) Equiratio cumulative distribution function matching as an improvement to the equidistant approach in bias correction of precipitation, *Atmospheric Science Letters*, **15** (1), 1–6. https://doi.org/10.1002/asl2.454.

Wang, H. -M., Jie Chen, J., Xu, C.-Y., Zhang, J. & Chen, H. (2020) A framework to quantify the uncertainty contribution of GCMs over multiple sources in hydrological impacts of climate change, *Earth's Future*, **8** (8), e2020EF001602. https://doi.org/10.1029/2020EF001602.

Wilby, R. L. & Keenan, R. (2012) Adapting to flood risk under climate change, *Progress in Physical Geography: Earth and Environment*, **36** (3), 348–378. https://doi.org/10.1177/0309133312438908.

Winsemius, H. C., Aerts, J. C. J. H., van Beek, L. P. H., Bierkens, M. F. P., Bouwman, A., Jongman, B., Kwadijk, J. C. J., Ligtvoet, W., Lucas, P. L., van Vuuren, D. P. & Ward, P. J. (2016) Global drivers of future river flood risk, *Nature Climate Change*, **6**, 381–385. https://doi.org/10.1038/nclimate2893.

Wu, X., Wang, Z., Guo, S., Liao, W., Zeng, Z. & Chen, X. (2017) Scenario-based projections of future urban inundation within a coupled hydrodynamic model framework: a case study in Dongguan City, China, *Journal of Hydrology*, **547**, 428–442. https://doi.org/10.1016/j.jhydrol.2017.02.020.

Yadav, N., Wu, J., Banerjee, A., Pathak, S., Garg, R. D. & Yao, S. (2024) Climate uncertainty and vulnerability of urban flooding associated with regional risk using multi-criteria analysis in Mumbai, India, *Environmental Research*, **244**, 117962. https://doi.org/10.1016/j.envres.2023.117962.

Yalcin, E. (2018) Generation of high-resolution digital surface models for urban flood modelling using UAV imagery, *WIT Transactions on Ecology and the Environment*, **215**, 357–366. https://doi.org/10.2495/EID180321.

Yalcin, E. (2019) Two-dimensional hydrodynamic modelling for urban flood risk assessment using unmanned aerial vehicle imagery: a case study of Kirsehir, Turkey, *Journal of Flood Risk Management*, **12** (S1), e12499. https://doi.org/10.1111/jfr3.12499.

Yalcin, E. (2020) Assessing the impact of topography and land cover data resolutions on two-dimensional HEC-RAS hydrodynamic model simulations for urban flood hazard analysis, *Natural Hazards*, **101**, 995–1017. https://doi.org/10.1007/s11069-020-03906-z.

Yalcin, E. (2024) Assessing future changes in flood frequencies under CMIP6 climate projections using SWAT modeling: a case study of Bitlis Creek, Turkey, *Journal of Water and Climate Change*, **15** (5), 2212–2231. https://doi.org/10.2166/wcc.2024.646.

Yanmaz, A. M. (2018) *Applied Water Resources Engineering*. Ankara: METU Press.

Zhang, L., Nan, Z., Yu, W., Zhao, Y. & Xu, Y. (2018) Comparison of baseline period choices for separating climate and land use/land cover change impacts on watershed hydrology using distributed hydrological models, *Science of the Total Environment*, **622–623**, 1016–1028. https://doi.org/10.1016/j.scitotenv.2017.12.055.

Zhou, Q., Leng, G. & Huang, M. (2018) Impacts of future climate change on urban flood volumes in Hohhot in northern China: benefits of climate change mitigation and adaptations, *Hydrology and Earth System Sciences*, **22** (1), 305–316. https://doi.org/10.5194/hess-22-305-2018.

First received 12 July 2025; accepted in revised form 19 November 2025. Available online 2 December 2025